UNIVERSITY OF TURKU

Impact of Solar Spectrum Variations on Current Matching in Perovskite-Silicon Tandem Solar Cells

Materials Engineering
Master of Science in Technology Thesis
Department of Mechanical and Materials Engineering
University of Turku

Author:
Helmi Vuorinen

23.4.2025
Turku

Master of Science in Technology Thesis

Subject: Materials Engineering
Author: Helmi Vuorinen
Title: Impact of Solar Spectrum Variations on Current Matching in Perovskite-Silicon Tandem Solar Cells
Supervisors: D. Sc. Aapo Poskela and D. Sc. Mahboubeh Hadadian
Number of pages: 82 pages
Date: 23.4.2025

Perovskite silicon tandem solar cells (PSTSCs) are a promising photovoltaic technology, as they can efficiently absorb light of multiple wavelength ranges, enabling efficiencies higher than perovskite and silicon solar cells alone. However, their long-term stability and operation in outdoor conditions remains a critical challenge. Current mismatch between the sub-cells, caused by spectral variations of incident light, can induce reverse-bias behaviour, and therefore degrade performance or even lead to cell breakdown. In this thesis, the stability of PSTSCs and the impact of spectral variations are considered through literature reviews of experimental aging and spectral studies, with the aim of understanding the gaps in current knowledge and guiding future research.

To evaluate the current matching conditions of PSTSCs, these conditions are modelled through spectral data under Finnish outdoor conditions. Absolute current mismatch increased with higher irradiance and was found to be generally higher on clear days than on cloudy days, while the relative current match was more stable around midday and showed higher variability during mornings and evenings. Seasonal differences were observed, with winter days showing the lowest mismatch and other seasons showing greater overall variability. These findings highlight the notable effects of environmental conditions on current matching and outline possible ways to minimize current mismatch in future tandem designs.

Key words: perovskite-silicon tandem solar cells, stability, current match, solar spectrum

Diplomityö

Pääaine: Materiaalitekniikka
Tekijä: Helmi Vuorinen
Otsikko: Auringon spektrin vaihtelun vaikutukset virran yhteensovitukseen perovskiitti-pii tandemaurinkokennoissa
Ohjaajat: TkT Aapo Poskela ja TkT Mahboubeh Hadadian
Sivumäärä: 82 sivua
Päivämäärä: 23.4.2025

Perovskiitti-pii tandemaurinkokennoja pidetään lupaavana aurinkosähköteknologiana, sillä niiden avulla voidaan absorboida tehokkaasti useiden eri aallonpituusalueiden valoa, mikä mahdollistaa paremman hyötysuhteen kuin perovskiitti- tai piiaurinkokennot saavuttaisivat yksinään. Niiden pitkäaikainen kestävyys ja käyttöikä erityisesti ulko-olosuhteissa ovat kuitenkin edelleen merkittävä haaste. Spektrin vaihteluista johtuva virran yhteensovituksen epäsuhtaisuus voi aiheuttaa virran kulkemista estosuuntaan, mikä heikentää kennojen suorituskykyä ja voi johtaa jopa niiden rikkoutumiseen. Tässä tutkielmassa tarkastellaan perovskiitti-pii tandemaurinkokennojen pitkäaikaista kestävyyttä sekä spektrin vaihteluiden vaikutusta kokeellisten ikääntymistutkimusten ja spektritutkimusten kirjallisuuskatsausten avulla. Tavoitteena on ymmärtää nykyisen tutkimuksen kehityskohtia sekä tunnistaa perovskiitti-pii tandemaurinkokennoille tarvittavaa tutkimusta tulevaisuudessa.

Perovskiitti-pii tandemaurinkokennojen virran yhteensovitusolosuhteiden arvioimiseksi tutkielmassa mallinnetaan erilaisia olosuhteita, kuten eri vuorokaudenaikoja ja vuodenaikoja, mitatulla spektridatalla suomalaisissa olosuhteissa. Virran yhteensovituksen epäsuhtaisuus kasvoi auringonsäteilyn kasvaessa ja oli yleensä suurempi kirkkaina päivinä kuin pilvisinä päivinä. Suhteellisen virransovituksen epäsuhtaisuus taas pysyi usein vakaana keskipäivällä, mutta vaihteli enemmän aamuisin ja iltaisin. Myös vuodenaika vaikutti merkittävästi tuloksiin. Talvipäivinä virran epäsuhtaisuus oli pienin muihin vuodenaikoihin verrattuna. Nämä havainnot korostavat ympäristöolosuhteiden merkittävää vaikutusta virran sovittamiseen ja havainnollistavat mahdollisia tapoja pienentää virran epäsuhtaisuutta tulevaisuuden tandemaurinkokennoissa.

Avainsanat: perovskiitti-pii tandemaurinkokenno, stabiilisuus, virran yhteensovitus, auringon spektri

Table of contents

Abbreviations

Si-SC	Silicon solar cell
PV	Photovoltaic
TCS	Tandem solar cell
PSC	Perovskite solar cell
PSTSC	Perovskite-silicon tandem solar cell
PCE	Power conversion efficiency
RB	Reverse bias
ETL	Electron transport layer
HTL	Hole transport layer
PERC	Passivated emitter and rear cell
SHJ	Silicon heterojunction
2T	Two-terminal
TCO	Transparent conductive oxide
FF	Fill factor
V_{OC}	Open-circuit voltage
4T	Four-terminal
PID	Potential induced degradation
MID	Moisture induced degradation
LeTID	Light and elevated temperatures induced degradation
UVID	UV-induced degradation
MPPT	Maximum power point tracking

RH	Relative humidity
$\boldsymbol{J_{sc}}$	Short-circuit current density
AM1.5G	Air mass 1.5 global
SZA	Solar zenith angle
$\boldsymbol{J_{ph}}$	Photocurrent density
EQE	External quantum efficiency
IQE	Internal quantum efficiency
SR	Spectral responsivity
LC	Luminescent coupling

1 Introduction

Due to the growing demand for electricity and the unsustainable use of fossil fuels, alternative energy sources are needed. Solar energy is considered one of the main renewable energy technologies to reduce dependence on fossil fuels and to meet the increasing energy demand [1],[2]. To date, solar energy accounts for only ~3% of global energy generation but is growing fast world-wide and is expected to meet ~20-30 % of global energy needs by 2050 [2]. Nowadays, silicon solar cells (Si-SCs) dominate the photovoltaic (PV) market due to their long-term reliability and high efficiencies [2]. However, their efficiency is approaching the theoretical Shockley-Queisser efficiency limit of 29.4% [3], making further improvements challenging. To overcome this limitation, new approaches are being researched.

In recent years, tandem solar cells (TSCs) have emerged as a promising technology. They consist of multiple single-junction sub-cells to form a high-efficiency tandem device. A tandem device can absorb different wavelength ranges of the solar spectrum, by combining solar cells with different band gaps [4], enabling efficiencies higher than single-junction cells. TSCs are being studied to overcome the efficiency limitations of single-junction Si-SCs, and perovskite solar cells (PSCs) have become a promising option for the top sub-cell due to their favourable properties. These properties include high efficiency, affordability, tunability and ease of fabrication [1],[5]. PSCs have been researched together with multiple solar cell technologies to form a TSC, such as organic solar cells, copper indium gallium selenide (CIGS) and silicon solar cells [1]. Perovskite-silicon tandem solar cells (PSTSCs) are considered to be the most promising, as the band gap of perovskite can be easily tuned to complement Si-SCs [1]. This enables more efficient conversion of sunlight, as the combination of high- and low-bandgap materials in TSCs allows absorption of a wider portion of the solar spectrum, from short to long wavelengths [6], therefore improving overall power conversion efficiency (PCE).

Despite the promising efficiency of PSTSCs, several areas still require further development to enable large scale commercialization and market adoption [7]. These challenges include, most importantly, the poor stability of perovskite sub-cells. Improving the stability, and therefore the lifetime of PSCs, would significantly advance the development of perovskite-silicon tandem cells. This thesis addresses the stability challenges from the perspective of the individual perovskite and silicon sub-cells, as well as within the tandem device. Accordingly, this thesis includes a literature review of aging experiments performed on PSTSCs. Based on the findings

of the literature review, the thesis aims to answer the first of its research questions: what type of experimental studies are still required for PSTSCs to bring them closer to commercialization?

In addition to stability concerns, the impact of spectral variations on perovskite-silicon tandem solar cells (PSTSCs) is another important but less studied research area. Since the sunlight reaching the Earth's surface varies with weather and time of the day, the shape of the incident light spectrum is not always the same [8]. These variations can significantly impact the power generation of PSTSCs, as the sub-cells absorb different wavelength ranges determined by their band gaps [9]. One of the most notable effects of spectrum variations is current mismatch. Current match refers to the condition in which the sub-cells in a tandem device operate at the same current [10]. Since the sub-cells are connected in series, the total current is limited by the sub-cell generating the lowest current. This can lead to reverse-bias (RB) conditions, where a sub-cell producing less current is forced into reverse voltage by the series connected tandem device [11]. RB can induce hot spots, resulting in power losses and potentially causing permanent degradation of the sub-cells [11]. Well current matched sub-cells reduce the possibility of RB conditions, thereby improving the overall stability of the tandem device.

Therefore, this thesis focuses on identifying when current mismatch occurs in PSTSCs using current-matching calculations based on Finnish spectral conditions. The spectral data were measured in Kupittaa, Turku, Finland, during 2025. Thus, the second research question addressed in this thesis is: How is current matching affected by changes in the solar spectrum? First, a literature review is presented to summarize previous spectral studies of PSTSCs, focusing especially on current matching, followed by the modelling approach used in the calculations.

Artificial intelligence (AI) was used to assist with grammar and phrasing, as well as to help in creating the code for the modelling part of this thesis. It was not used to write or generate the text, conclusions, or analyses of the thesis.

2 Overview of Perovskite-Silicon Tandem Solar Cells

2.1 Perovskite Solar Cells, Silicon Solar Cells, and Perovskite-Silicon Tandem Solar Cells: Properties and Key Challenges

With about 95% market share in 2020, silicon solar cells are by far the most widely used photovoltaic (PV) technology [12]. Silicon solar cells (Si-SCs) have excellent optical properties [13], enabling them to achieve high power conversion efficiency (PCE). They also exhibit long operational lifetime, with typical modules retaining at least 80% of their stability for up to 25 years field operation [10]. The most common silicon solar cell architectures include aluminum back surface field (Al-BSF), passivated emitter and rear cell (PERC), tunnel oxide passivated contact (TOP-Con) and silicon heterojunction (SHJ) solar cells [1],[12]. Si-SC fabrication has progressed from basic p-n junctions to more complex and efficient crystalline silicon technologies [14]. Surface texturing and passivation layers have significantly increased the efficiency of Si-cells by enhancing light trapping and reducing recombination losses [15]. However, one of the main disadvantages of Si-SC production is the energy-intensive and polluting processes involved in purification and crystallization of silicon [15],[16]. More recently developed cell architectures such as silicon heterojunction (SHJ), often used in perovskite-silicon tandem solar cells, are fabricated at temperatures below 250°C, in contrast to technologies like PERC or Al-BSF Si-SCs, which involve higher temperatures [15]. While advanced architectures such as SHJ enable low-temperature processing, Si-SCs are still approaching their theoretical limits of power conversion efficiency, meaning alternative solutions are being studied to overcome this issue [10].

Perovskite solar cells have gained significant attention in recent years, due to their low-cost processing, high efficiencies and adjustable band gap among other advantages [4],[13],[17]. However, their large-scale commercialization is still hindered by their poor long-term stability. Perovskite solar cells are typically composed of a top and back electrode, an electron transport layer (ETL), hole transport layer (HTL) and an active perovskite layer [18]. The active layer consists of a perovskite material with the general crystal structure of ABX_3 [17]. In the formula, A and B stand for cations, and X stands for anion [17]. The most common perovskites used in PSCs are methyl-ammonium-lead-iodide ($MAPbI_3$) and formamidinium-lead-iodide ($FAPbI_3$) [17]. The most common fabrication techniques of perovskite solar cells (PSCs) include spin-coating processes, which can be difficult to implement on a large scale [13]. However, techniques such as slot-die coating, spray coating, and blade coating have been developed to

enable scalability [13]. Yet they present their own challenges, especially in tandem structures. This is due to the textured surface often used in silicon solar cells (Si-SCs), which hinders the deposition of the perovskite layer [10]. While a polished surface benefits perovskite deposition, it reduces the effectiveness of light-trapping strategies in Si-SCs [10].

Despite the favourable properties of PSCs, their large-scale commercialization is still hindered by their instability and toxicity of certain materials, such as lead [10]. Current research focuses on developing safer and more stable perovskites through alternative compositions and encapsulation. Furthermore, in response to the power conversion efficiency (PCE) limits of Si-SCs, perovskite-silicon tandem solar cells (PSTSCs) present a promising approach, though several aspects still require further research before these devices can be commercially available.

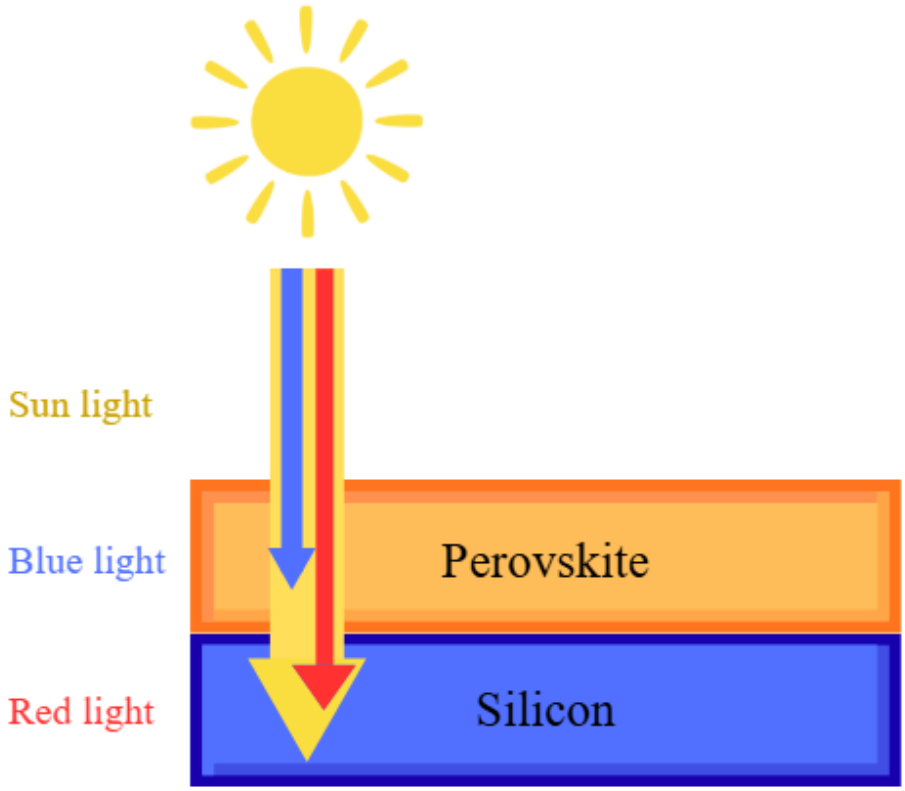

Figure 1. Light absorption in perovskite-silicon tandem solar cells (PSTSCs) with yellow arrow indicating the sun light, blue arrow the blue part of the incoming sun light and red arrow the red part of the incoming sun light. Figure inspiration from [19],[20].

The tandem structure of perovskite-silicon tandem solar cells (PSTSCs) enables more efficient light conversion compared to single-junction solar cells by utilizing the solar spectrum more efficiently, also allowing fewer thermal losses caused by excess photon energy wasted as heat [4],[13]. In this architecture, the perovskite top cell absorbs light primarily in the visible region, while the silicon bottom cell focuses on capturing the near-infrared light passing through the

perovskite layer (Figure 1) [9]. This allows a larger portion of the solar spectrum to be converted into electricity compared to single-junction cells [21].

Since the active layers absorb light at different wavelengths of the solar spectrum, an optimal combination of 1.12 eV band gap for the crystalline silicon bottom cell and 1.65-1.70 eV band gap for the perovskite top cell can theoretically achieve efficiencies of up to 46% [22]. To date, perovskite-silicon tandem solar cells (PSTSCs) have achieved efficiencies as high as 34.9 %, which is significantly higher than the efficiencies of these sub-cells: about 27.0 % for perovskite, and 27.6 % for crystalline silicon single-junction solar cells in 2025 [23]. To further increase the efficiency, it is important to consider various performance losses, while also optimizing the band gap so that the solar spectrum can be utilized as efficiently as possible [22]. PSCs combine a tunable band gap with a variety, generally low-temperature fabrication techniques, which makes their manufacturing relatively simple and flexible [4],[24]. The composition of perovskites can be modified for different architectures, making perovskites ideal light-absorbing materials for TSCs, allowing their light absorbing properties to be tailored to specific applications [4]. Table 1 provides an overview of silicon, perovskite, and perovskite-silicon tandem solar cells and their key properties.

Table 1. Key properties of silicon, perovskite, and perovskite-silicon tandem solar cells. Cell architecture figure inspiration from [25] for silicon heterojunction (SHJ) solar cell, from [26] for perovskite solar cell (n-i-p), and from [1],[27] for perovskite-silicon tandem solar cell. SHJ architecture was chosen to present the silicon solar cell here because it is considered the most suitable for PSTSCs.

Category	**Silicon solar cells (Si-SCs)**	**Perovskite solar cells (PSCs)**	**Perovskite-silicon tandem solar cells (PSTSCs)**
Lab-scale PCE (%)	27.6 [23]	27.0 [23]	34.9 [23]
Lifetime	Can retain over 80% of their efficiency for 25 years [10]	~ 1 year [28]	Limited by PSC, ~ 1 year [28]
Light absorption	Near theoretical maximum [10], lower absorption of low energy photons [9]	Tunable band gap [17]	Utilizes solar spectrum more efficiently compared to single-junction cells [4]
Optical losses	Reflection and parasitic absorption [4]	Reflection and parasitic absorption [29]	Reflection and parasitic absorption [4],[1]
Electrical losses	Negligible, but exists (interconnection layer and mismatch losses) [30]	High series resistance, recombination losses [31]	Current-matching, FF, and V_{OC} losses [1]
Environmental concerns	Recyclability [32]	Lead toxicity [10] and recyclability [33]	Lead toxicity [10] and recyclability [32],[33]
Scalability	Scalable	Under research	Under research
Architecture **Silicon: SHJ** **Perovskite: n-i-p**	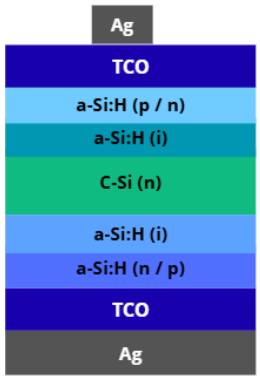	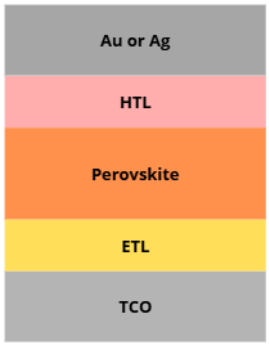	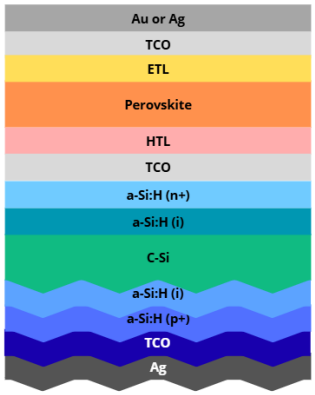

As can be seen in Table 1, optical losses are present in all three of the solar cell technologies, but the stacked architecture of tandem devices introduce additional optical losses due to increased number of layers in these cells. The optical losses present in these technologies are usually categorized in two: reflection and parasitic absorption losses [1],[4]. Parasitic

absorption losses are caused when light is absorbed outside the active layer, resulting in fewer photons available for current generation and PCE [1],[4]. In monolithic devices, such as two terminal (2T) tandem structures, this occurs mainly in the hole transport layer (HTL) of PSCs, and the interconnecting layer (ICL) between the sub-cells [1]. Reflection losses, on the other hand, happen when light is reflected away from the surface or internal interfaces of the devices cell due to different refractive indexes, leading to reduced PCE [1].

Various studies have been conducted to minimize the optical losses in perovskite-silicon tandem solar cells (PSTSCs). Solutions to mitigate the reflection losses include an interconnecting layer with refractive index between that of perovskite and silicon sub-cells (2.4, and 3.7, respectively) [1]. For example, Mazzarella et al. deposited nanocrystalline silicon oxide (nc-SiO_x: H) as the interconnection layer to improve light capture in the bottom sub-cell [34]. The refractive index (~2.6 at 800 nm) was found to reduce the reflection losses in the near-infrared region [34]. Other possible solutions include modifying the refractive index of the transparent conductive oxide (TCO), applying an antireflective coating, and using textured surface for the silicon sub-cell [1]. Approaches that reduce reflection losses are often closely linked to the reduction of parasitic absorption losses. For instance, transparent conductive oxides (TCOs) such as indium tin oxide (ITO) can absorb light and therefore limit photon transmission to silicon bottom cell [11]. Replacing ITO with materials such as zinc tin oxide (ZTO), which has a better matching refractive index to the perovskite and silicon layers, can help mitigate optical losses [4],[1]. Furthermore, the use of antireflective coatings and surface texturing of the silicon bottom-cell can help minimize these losses, since flat surfaced silicon cells are known to have the most optical losses [4],[1]. This, however, is not without challenges, as surface texturing can create difficulties in the fabrication process of PSTSCs [1].

Beyond instability and optical losses, the commercialization of PSTSCs is limited due to electrical losses. In this work, current matching is the most relevant electrical loss mechanism, which refers to the requirement for the upper and lower sub-cells to generate the same current, and will be discussed in more detail in the following sections. Other electrical loss mechanisms include losses in fill factor (FF) and open-circuit voltage (V_{OC}) [1]. Like current matching, fill factor losses are mainly influenced by electrical contact quality, as poor contacts lead to higher resistive losses [1]. However, other factors also play a significant role, including the optimization of layer thicknesses and the enhancement of charge transport rate in the ETL and HTL through doping [1]. This is because these factors determine the contact quality between the sub-cells and the series resistance and thus affect the fill factor [1]. Moreover, V_{OC} losses

are mainly related to perovskite sub-cell instability, which arises from factors such as phase transformations and defects [1]. Besides improving perovskite stability, better energy level alignment between the perovskite layer and charge transport layers (ETL and HTL) is needed to reduce V_{OC} losses, as misaligned energy levels can cause inefficient charge transformation [1].

In summary, the performance and commercial viability of PSTSCs is still limited due to various factors, such as instability, optical and electrical losses. While improvements in device architecture and layer optimization may significantly improve device efficiency, major improvements need to be made regarding perovskite's stability. Moreover, material choices, such as replacing lead-based perovskites, are crucial for developing more sustainable and environmentally friendly solar cell technologies.

2.2 Structure and Performance of Perovskite-Silicon Tandem Solar Cells

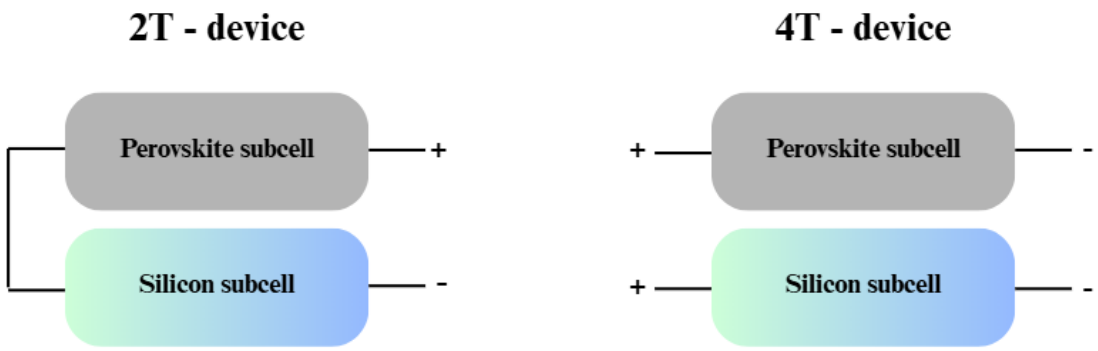

Figure 2. On the left side, two-terminal (2T) tandem device structure and on the right side a four-terminal (4T) device structure.

Perovskite-silicon tandem solar cells (PSTSCs) consist of two sub cells, that are the perovskite top cell and silicon bottom cell [6]. The most common tandem cells are monolithic two-terminal (2T) tandems (Figure 2), in which the sub cells are stacked on top of each other and connected in series internally [10],[35]. In the case of perovskite-silicon tandems, the perovskite sub cell is on top and silicon sub cell is underneath, allowing the different wavelength of sunlight to be utilized as efficiently as possible [10]. The solar spectrum effects will be discussed in more detail in Section 3.2. There are two main 2T-configurations: n-i-p and p-i-n. The naming depends on which transport layer is deposited first: in n-i-p structures, the hole transport layer is deposited first, while in p-i-n structures, the electron transport layer is deposited first [36].

Two-terminal configurations are usually fabricated by placing the perovskite layer directly on top of the silicon layer [36]. One of the key components of 2T devices is their interconnection layer, which connects the perovskite and silicone layers electrically to each other [35]. The interconnection layer is often either a conductive layer, such as zinc-doped tin oxide (ZTO) or aluminum-doped zinc oxide (AZO), or doped tunnel junction layer, typically a highly doped $n^{++}Si/p^{++}$ Si junction [35].

For current generation, the energy of the incident photons must be higher than that of the band gap energy of the absorber layers [37],[38]. When photons with proper energy are absorbed, it causes the valence electrons to excite to the conduction band, creating electron-hole pairs [37]. The generated carriers are then separated by the internal potential within the solar cell [38]. Electrons are transported towards the electron transport layer (ETL) and holes to the hole transport layer (HTL) [38]. The carriers are then collected at the electrodes, producing current in the external circuit [37],[38].

In two-terminal PSTSCs, the perovskite top cell and silicon bottom cell generate charge carriers independently. The sub-cells are electrically connected through an interconnecting recombination layer (ICL), which connects the sub-cells in series (Figure 3). The function of the ICL is to enable charge recombination at the interface between the silicon and perovskite sub-cells. In the ICL, the charge carriers from the perovskite sub-cell recombine with the charge carriers from the silicon sub-cell, allowing current to flow through the device. As the architecture in 2T PSTSCs forms a series connection through the ICL, the current of the tandem device is limited by the sub-cell generating the lower current, while the total voltage is the sum of the voltages of the two sub-cells. [39]

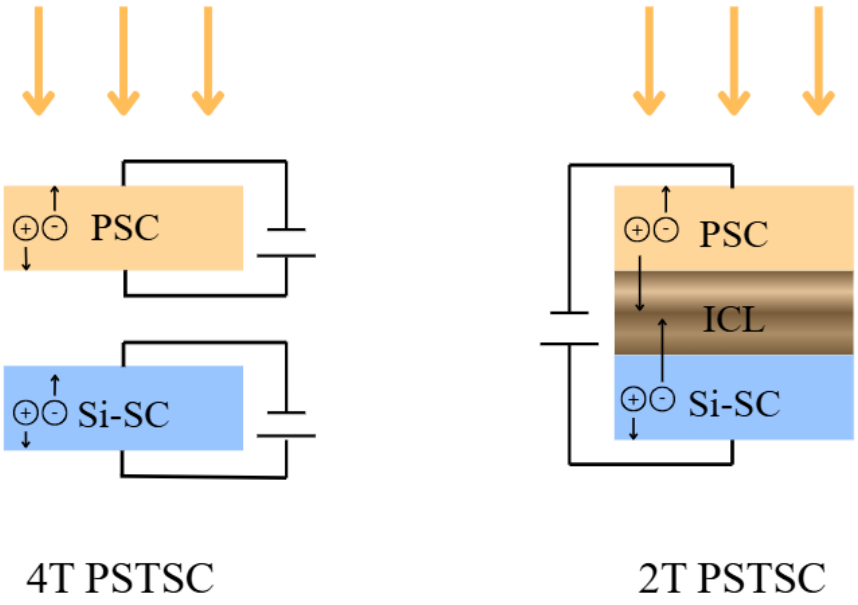

Figure 3. Comparison of four terminal (4T) and two terminal (2T) perovskite-silicon tandem solar cells (PSTSCs), with yellow arrows indicating incoming sunlight. The 4T architecture allows the sub-cells to operate electrically independently, while in the 2T configuration the interconnection layer (ICL) connects the sub-cells in series, requiring current matching in the device.

Another common option is four-terminal (4T) tandem cells, in which the top and bottom cells operate independently, each with its own electrical contacts [1],[35] (Figure 2). Therefore, the fabrication is usually carried out by separately preparing the perovskite and silicon sub cells and only connecting them optically [35]. The sub cells are then mechanically stacked on top of each other, meaning that the structure does not require current or voltage matching as in 2T cells [10],[21].

Both configurations (2T and 4T) have their own advantages and disadvantages when applied to perovskite-silicon tandem solar cells (PSTSCs). Two terminal devices require fewer fabrication steps [35] and use less material compared to four terminal devices. However, in 2T configurations, the overall device lifetime is limited by the less stable perovskite sub cell, since the cells are electrically connected [35]. This means that when the perovskite sub-cell degrades, it reduces the current through the whole tandem device [35]. Due to the series connection between the sub-cells, the 2T configuration requires current matching, unlike the 4T configuration [36]. Four terminal PSTSCs, due to their electrically independent nature, are considered more stable than 2T cells under conditions such as solar spectrum variations [10]. They can utilize a wider range of the solar spectrum without current matching limitations, which may lead to higher overall power generation compared to 2T-devices [35]. Additionally, the structure enables easier maintenance of these devices, since the broken sub cell can easily be replaced [35]. However, the optical losses caused, for instance by absorption in the transparent

conductive oxide (TCO), are smaller in 2T-devices, as there are fewer optical layers compared to the optically stacked 4T devices [35].

As mentioned, a perovskite-silicon tandem solar cell (PSTSC) consists of a wider band gap perovskite top cell stacked on a lower band gap silicon bottom cell [9]. This configuration enables more photons to be absorbed, as high energy photons are absorbed by perovskite sub-cell and lower energy photons by the silicon sub-cell [9],[38]. As current matching is required only in two-terminal (2T) tandem devices, where the sub-cells are connected in series [36], the following sections primarily focus on this configuration.

2.3 Stability Challenges of Perovskite and Silicon Solar Cells

2.3.1 Perovskite solar cell degradation

Perovskite solar cell instability remains one of the main factors preventing the large-scale commercialization of perovskite-silicon tandem solar cells. The stability issues often arise from the degradation of the perovskite layer [40], which is usually accelerated by external factors, such as high temperatures, oxygen and moisture [41]. The stability issues can be divided into internal and external factors [41]. Internal instability is caused by the intrinsic instability of the perovskite material itself, while external instability by environmental factors [41].

The intrinsic instability is closely linked to perovskite's crystal structure [40]. The cell is particularly vulnerable to structural changes in the perovskite layer, as these can significantly affect its optoelectronic properties and consequently, the cell performance [42]. To improve the internal stability, the structure of perovskite can be altered by substituting organic cations such as methylammonium (MA) with alternatives like formamidinium (FA), or by adding inorganic cations to the perovskite structure [40]. Alternative ions to eliminate MA has been shown to improve the resistance to oxygen and therefore enhance the overall stability of the perovskite solar cells [40]. Another common internal factor causing instability is ion migration in the crystal structure of perovskite. Under electric field or light exposure, iodide ion vacancies in the perovskite layer can migrate through the perovskite crystal towards interfaces, causing effects such as hysteresis in the cells. Hysteresis refers to the phenomenon in which the measured current-voltage curves depend on the scan rate and direction, resulting in differences between forward and reverse scans. However, the exact effects of ion migration on device performance are still under research. [43]

Environmental stressors, including humidity, illumination and oxygen, can induce significant degradation phenomena in perovskite solar cells [41]. In the presence of oxygen, the organic components of the perovskite layer can be oxidized [42]. In the dark, however, little to no degradation occurs [42]. When both oxygen and light are present in the perovskite layer, significant degradation can take place, as light promotes photo-oxidation, leading to the formation of superoxide and accelerating the degradation process [41]. Beyond photo-oxidation, exposure to light can induce halide segregation and compositional changes in the cells [41],[44]. Some of these changes are permanent, reducing cell efficiency, or reversible, as in the Hoke effect, where halide ions segregate under illumination but revert once the light is removed [44]. Another external factor causing stability issues in PSCs is moisture [41]. Moisture can easily diffuse into the perovskite layer, leading to the formation of hydrogen bonds [41]. These chemical reactions between water and perovskite can accelerate degradation by modifying its crystal structure and reducing its light absorbing properties, thereby decreasing the performance of the cells [41].

To mitigate the stability issues, extensive research has been conducted on perovskite solar cell encapsulation [42],[45]. For effective encapsulation, the encapsulant must prevent the ingress of moisture and oxygen, while being chemically compatible and non-reactive with other parts of the cell [5]. The most widely used encapsulants for PSCs include materials such as thermoplastic polyolefins (TPOs) [45], polyolefin elastomers (POE) [46], thermoplastic polyurethanes (TPUs) [47] and polyisobutylene (PIB) [45]. To enable the commercialization of PSCs while maintaining low-cost production and simple fabrication, the encapsulants should be affordable, easy to apply and capable of providing effective device protection for improved lifetime of the cells.

2.3.2 Silicon solar cell degradation

Silicon solar cells already have comparatively good stability, as they can maintain up to 80% of their original efficiency for up to 25 years [4]. However, several factors can affect their degradation including delamination, colour changes, corrosion and environmentally induced degradation, with corrosion and discoloration considered the most common [48]. Corrosion in silicon solar cells can occur when moisture enters the device, either through the edges of the module or through cracks formed during transportation, handling or installation [48],[49]. This can cause degradation of the metal contacts, which in turn can promote increased leakage current of the device [48]. It can also lead to diffusion of aluminum (Al) and sodium (Na) ions

from the module's aluminum frame and glass, which can promote potential induced degradation (PID) [49]. The main cause of PID is often associated with the migration of sodium ions from the soda-lime glass [50]. Under high system voltage, these ions drift through the encapsulation layer to the silicon surface, where they interact with defects, leading to increased leakage current and power losses [50]. Moisture induced degradation (MID) in the silver grid or encapsulation layer can lead to various effects in the cells, such as altered optical properties, reduced charge generation or increased series resistance [49]. Additionally, corrosion in Si-modules can cause degraded adhesion of the components, also known as delamination. Delamination often occurs either between the encapsulant and the cells or the encapsulant and the front glass [48]. It can lead to increased light reflectance, higher water ingress and, if it happens near the edges, increase the probability of electrical risks [48].

In addition to moisture induced degradation, other environmental factors, such as high temperatures, UV and visible light, can affect the degradation of silicon solar cells on long-term. Light and elevated temperature induced degradation (LeTID) can cause performance losses of up to 16% in multicrystalline silicon solar cells [51]. Although the reasons for LeTID are not fully understood, studies suggest that it might be due to metal impurities or hydrogen within the cells, which can cause bulk and surface defects in the cells when exposed to elevated temperatures and light [51]. Choosing appropriate materials and controlling material thickness can help to mitigate LeTID [51]. UV-induced degradation (UVID), on the other hand, is primarily related to color changes in the module, which are often linked to changes in the encapsulant material's transmittance [52],[53]. This discoloration due to moisture permeation or UV exposure may affect the photovoltaic properties of the module, leading to decreased power output, as less light transmits into the cell [52]. In addition, bubbles can be formed as a result of chemical reactions within the cells, which can cause scattering of the incoming light and therefore negatively affect the power generation of the cells [8]. Light induced effects can be controlled by using suitable materials in the module, for instance with encapsulants that have altered UV-properties or special glass covers, such as cerium contained glass [53].

2.3.3 Degradation mechanisms for perovskite-silicon tandem solar cells

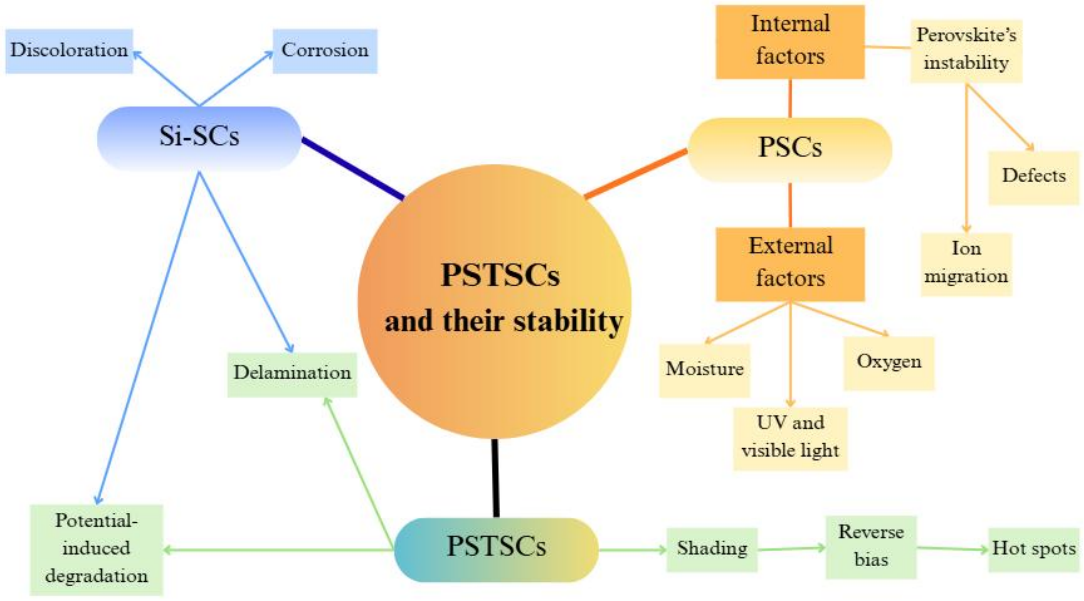

Figure 4. Perovskite-silicon tandem solar cells (PSTSCs) and their degradation mechanisms, on cell level (perovskite (PSCs) and silicon (Si-SCs)), and as a tandem cell.

Since silicon solar cells are significantly more stable, most of the stability challenges in perovskite-silicon tandem solar cells arise from perovskite sub-cell instability. At cell level, factors like electrode design, current and thermal coefficient mismatching can negatively impact stability [7]. The electrode design can significantly affect the lifetime of tandem devices, especially the perovskite sub-cell. Electrodes made of silver (Ag) or gold (Au) tend to diffuse into the perovskite layer, leading to degradation of the cells [7]. Ag or Au electrodes can be replaced, for instance, with carbon-based alternatives, which can not only mitigate degradation but also reduce hot spot formation in the cells [7]. Apart from material choices, it is important that the electrodes are both conductive and transparent, depending on the device design [7]. For four-terminal (4T) tandems, three transparent electrodes are needed (Figure 5), which increases fabrication costs [54]. The transparency and conductivity of the top cell electrodes are crucial, since the near-infrared photons need to reach the bottom sub-cell through the upper cell [54]. The conductivity of the electrodes is important, as it makes the charge collection easier on the upper perovskite sub-cell. One solution for improved electrode design, especially in 4T devices, could be a thin metal electrode made of gold (Au) and chromium (Cr) [54].

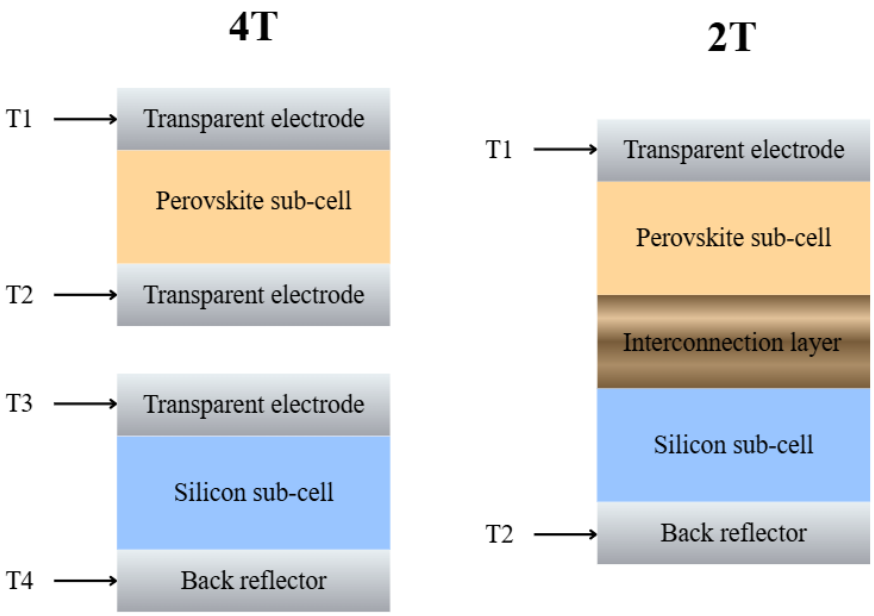

Figure 5. Four-terminal (4T) and two-terminal (2T) perovskite-silicon tandem solar cell electrode design. Figure inspiration from [55].

Due to the brittleness of perovskite, it is highly sensitive to mechanical stress [7]. A mismatch in thermal expansion coefficients between the perovskite and silicon layers can further increase this stress, negatively affecting the stability of the tandem cells [7]. The range of different thermal expansion coefficients can cause delamination in the cells, which is one of the key factors contributing to module failure [7],[56]. Delamination can occur in different layers of the cell, such as encapsulant, back sheet or glass [56]. It is particularly significant during thermal cycling, for instance when day to night temperature variation is notable. In addition to delamination induced degradation in cells, the textured surface of the silicon bottom cell imposes additional challenges. The textured surface is included in the cell structure to enhance light capturing in the silicon sub-cell. While this improves optical absorption, it also increases mechanical stress due to stress concentrations at the textured surface and makes the fabrication of TSCs more challenging. In particular, the deposition of the perovskite layer becomes more difficult, as achieving full surface coverage on the textured surface is harder. To mitigate the mechanical stress caused by the different thermal expansion coefficients, one potential solution is to lower the crystallization temperature during annealing, a heat treatment used to form the perovskite crystal structure, which can help reduce the thermal strain between the layers. Additionally, optimizing the thermal expansion coefficients and choosing a suitable encapsulant with a low elastic modulus could be an option in preventing delamination in the modules. [7]

In two-terminal (2T) tandem devices, current matching refers to the generation of equal current in both sub-cells, achieved through a balanced distribution of light absorption between the sub-cells [10]. If the sub-cells absorb light in a way that leads to unequal photocurrent generation, current mismatch occurs [10]. It can cause up to 10% efficiency losses when the devices are operating at real world conditions [10]. For instance, if the upper perovskite sub-cell absorbs more light, less light reaches the silicon bottom cell. Due to series connection, the total current of the device is then limited by the lower current of the silicon sub-cell [1],[10], meaning that any excess current generated by the other sub-cell cannot be utilized. Current matching is strongly affected by changes in the solar spectrum, as the sub-cells absorb different wavelength ranges [10]. As a result, variations in the spectrum can lead to current mismatch in perovskite-silicon tandem solar cells (PSTSCs), as can be seen in Figure 6.

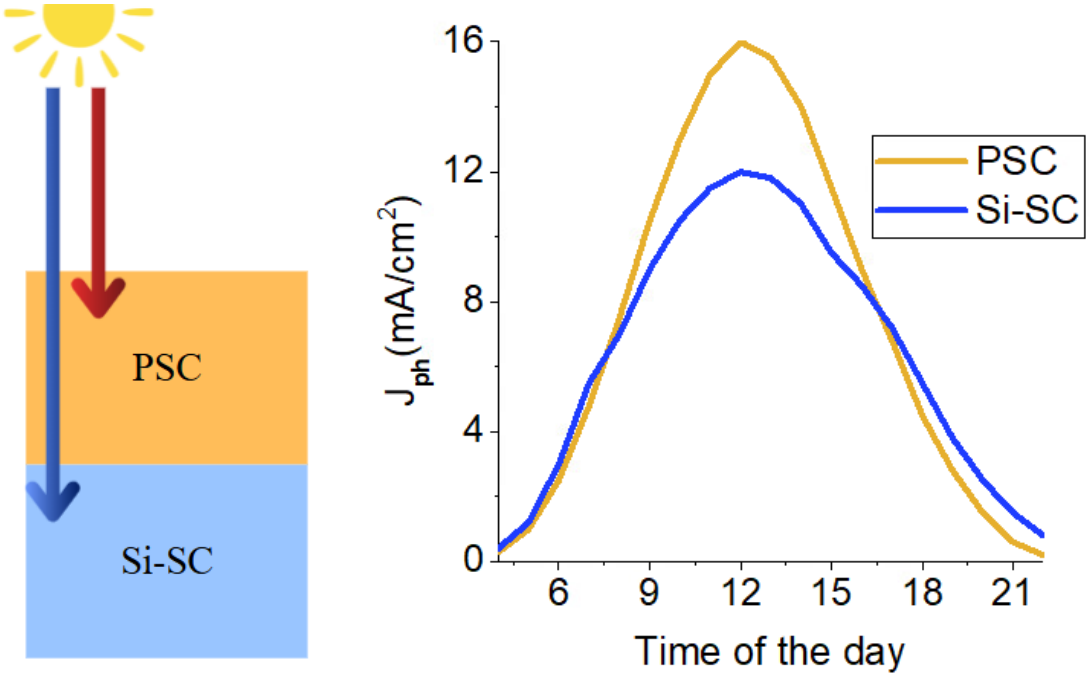

Figure 6. Current mismatch in two-terminal perovskite-silicon tandem solar cells. On the left side, the plot shows a mismatched case, where the perovskite sub-cell produces higher photocurrent, particularly around midday, leading to current mismatch.

Ideally, the ratio of the photocurrent densities should be close to one, so that the photocurrent generated in the sub-cells is well matched. Figure 6 shows an unideal case, where the perovskite sub-cell produces higher photocurrent around midday, leading to increased mismatch values. To achieve better current matching, the band gap combination in perovskite-silicon tandem solar cell can be optimized by tuning the properties of the perovskite absorber [21],[57]. As the current matching is so closely linked to solar spectrum variations, it will be discussed in more detail in Section 3.2.

Although current mismatch itself does not directly cause degradation, it can result in reverse-bias (RB) and hot-spot formation, which can accelerate device degradation [10]. RB can occur in series connected cells when one of the cells restricts the current flow through the string [11],[58]. This can happen, for instance, due to partial shading from nearby objects such as trees [2]. Shading of one or more cells prevents them from generating the same current as the unshaded cells [2]. As a result, the shaded cell limits the current of the entire series-connected string and may be forced into reverse-bias operation, meaning that the voltage across the cell reverses [2]. RB can induce irreversible changes in the cells and create uneven heat distribution, leading to the formation of hot spots in the cells and possible power losses [11],[58]. Solutions for mitigating reverse bias include bypass diodes [11],[58],[2], modifying the band gap of perovskite sub-cell and reducing the number of cells in a string [11]. However, these approaches also present challenges. Due to the low breakdown voltage of PSCs, the amount of bypass diodes needed would increase the overall module cost significantly [11]. Therefore, the most important way to mitigate RB behaviour, would be to current match the tandem device well. This could be done by modifying the light absorbing layers [59], adjusting the band gap [7], or modifying the overall tandem cell configuration [10],[60]. Reverse bias behaviour and band gap tuning of PSTSCs is discussed in more detail in Section 3.2.

At module level, factors contributing to degradation are reflection losses, potential induced degradation (PID), and delamination [7]. As mentioned in silicon solar cell degradation mechanisms, PID refers to a process in which ions, such as sodium, migrates into the light absorbing layers, leading to cell degradation [7]. Although PID occurs in both silicon and perovskite solar cells, the mechanisms differ significantly. In PSCs PID is mainly related to ion migration in the perovskite layer [61]. This ion movement can induce defects such as vacancies and accelerate phase segregation and decomposition, leading to decreased device performance [61]. Since tandem modules can experience potential differences ranging from -500 V to +500 V, these voltage differences can induce ion migration from materials such as antireflective coatings, encapsulants, and active layers, leading to power losses in the devices [7],[62]. In a study conducted by Xu et al., potential induced degradation was observed to affect only the perovskite sub-cell [62]. Therefore, introducing materials that block ion migration into or out of the perovskite layer could help mitigating the potential induced degradation [62]. These materials could either be used an encapsulant to block the ion migration, or it could involve modifying the perovskite structure to suppress ion movement within the layer [7].

2.3.4 Other performance losses

Apart from long-term degradation mechanisms, other factors can affect the performance of solar cells more rapidly, whereas degradation processes typically develop gradually over time [63]. These factors refer to processes such as soiling, hot spot formation, junction box failures or lightning strikes [63], and often take place suddenly and can cause an immediate decline in performance of the modules. Soiling, usually caused by dirt, snow or leaves blocking the sunlight, can cause significant changes in photovoltaic properties of PV modules by shading the cells [64]. If the cells are only partially shaded, the affected areas can heat up, promoting hot spot formation [64]. This can cause permanent damage to the cells if bypass diodes are not used [64]. In addition, hot spots form as a result of short-circuited cells or cracks in the cells [63]. Another potential cause of sudden degradation in solar cells are lightning strikes, which can cause changes in the electrical properties of the modules, such as efficiency losses or reduced power output due to high voltages passing through the PV system [63].

2.4 Literature Review of Aging Experiments

To date, aging studies have primarily focused on single-junction perovskite solar cells (PSCs), with only a limited number of studies targeting perovskite-silicon tandem solar cells (PSTSCs). The focus has been on improving PSC stability, which is also a key factor for tandem solar cells' long-term reliability. Generally, aging tests are performed to study the long-term behaviour of solar cells under controlled conditions. Some commonly used accelerated aging tests for PSCs include damp heat test and light soaking, which usually last for 1000 hours [17]. In some light soaking tests, here referring to tests that examine the durability of cells under UV and visible light, the duration was limited to around 300 hours [7], which is too short to reliably assess long-term operation under real-world conditions since these devices are designed to operate for multiple years. Light soaking is usually combined with maximum power point tracking (MPPT), where the cells operate at their maximum power point [65]. This provides insight of the real-world working conditions, where the cells need to operate at their maximum power point. Since perovskite solar cells are sensitive to moisture and high temperatures [40], another aging study that is often conducted is a damp heat test. Damp heat test is usually conducted by subjecting the cells in 85% relative humidity (RH) and 85°C for 1000 hours [66],[67] to evaluate how the cells withstand high temperatures and humidity [68].

Another way to study the thermal properties of the cells is through a thermal cycling test, where the cells are subjected to repeated temperature variations between -40°C and 85°C [68]. Thermal cycling is used to determine whether temperature variations cause delamination or other failures in the cells [68]. In addition, outdoor aging tests are performed to see how cells perform under real outdoor conditions, such as varying spectra, temperature and humidity [69]. Table 2 shows various aging studies, their conditions and their effects on the initial performance of perovskite-silicon tandem solar cells.

Table 2. Literature review of aging experiments performed on perovskite-silicon tandem solar cells, with cell type, aging test conditions and effect on cell performance.

Cell type	Test type	Test conditions	Effect on initial efficiency	Other	Ref.
Monolithic 2T perovskite/SHJ-Si tandem	Damp heat test	1000h at 85% RH and 85°C	10% degradation in performance	No encapsulant, ALD deposited tin oxide buffer layer	[66]
Monolithic 2T perovskite/SHJ-Si tandem	Damp heat	1000h, 85°C and 85% RH	Minimal performance loss	TPU and TPO encapsulated	[67]
Monolithic 2T perovskite/SHJ-Si tandem	Damp heat	1000h, 85°C and 85% RH	Retained 95% of its initial performance	Butyl rubber as an edge sealant	[70]
Monolithic 2T perovskite/SHJ-Si tandem	Thermal cycling	50 thermal cycles (-40°C to 85°C)	Minimal performance loss	TPU and TPO encapsulated	[67]
Monolithic 2T perovskite/SHJ-Si tandem	Thermal stability	400h, 85°C, 40-50% RH in dark	Retained their initial performance	Butyl rubber as an encapsulant	[71]
Monolithic 2T perovskite/SHJ-Si tandem	MPPT	400h, 40°C, 40-50% RH under 1-sun	Retained their initial performance	Polyolefin (POE) as an encapsulant	[71]
Monolithic 2T perovskite/SHJ-Si tandem	Thermal stability	From 25°C to 85°C and cooled back to 25°C, 200 min	Retained their initial performance	Without encapsulant	[72]
Monolithic 2T perovskite/SHJ-Si tandem	MPPT	Under AM1.5, 25°C, 30-40% RH for 300h	Retained 95% of the initial performance	Without encapsulant	[72]
Monolithic 2T perovskite/SHJ-Si bifacial tandem	Outdoor aging	Outdoor conditions (Saudi-Arabia), six months	V_{OC} and J_{SC} retained their initial values, FF decreased from 80% to 50%	Butyl rubber as edge sealant	[69]
Monolithic 2T perovskite/SHJ-Si tandem	Outdoor aging	Hot and humid environment, ~100% RH for 43 days	Retained over 90% of the initial performance	Butyl rubber as an edge sealant	[73]
Monolithic 2T perovskite/SHJ-Si tandem	Damp heat	85% RH and 85°C for 500h	Retained 87% of initial performance	Butyl rubber as an edge sealant	[73]
Monolithic 2T perovskite/SHJ-Si tandem	MPPT	250h under 1-Sun illumination	Maintained the original performance	Butyl rubber as an edge sealant	[73]

Most of the aging studies done for perovskite-silicon tandem cells have been conducted using monolithic two terminal (2T) silicon heterojunction (SHJ) tandems (Table 2). In a study conducted by Bush et al. a damp heat test (1000 h, 85°C and 86% RH) was done to enable more efficient and stable tandem devices [66]. The tandem devices were unencapsulated, but a tin oxide buffer layer was deposited using atomic layer deposition (ALD) to protect the perovskite layer and minimize optical losses [66]. There was a 10 % decrease in the performance of the tandem devices during the testing [66]. However, the devices reached efficiencies of 23.6%, which is more than the sub-cells could achieve alone [66]. In addition, measuring the efficiency of the perovskite sub-cell alone after testing could help determine how much of the total degradation is caused by the perovskite cell itself but it is often inaccessible in this way [72] as the sub-cells are monolithically connected and cannot be measured separately after fabrication. An interesting aspect would be to study how the devices would perform under the same conditions if an encapsulant, such as EVA or POE, was used.

In another study Toniolo et al. did a similar damp heat test (85°C and 85% RH) for 1000 hours where the cells were encapsulated using thermoplastic polyurethane (TPU) and thermoplastic polyolefin (TPO) [67]. Additionally, the cells were subjected to thermal cycling, where 50 thermal cycles from -40°C to 85°C was performed [67]. Two different tests were performed as the damp heat test assessed moisture-induced degradation and thermal cycling the stability under fluctuating temperatures. The cells showed minimal performance loss in both tests, indicating good stability under high humidity and temperatures [67]. Similarly, in other studies the damp heat performance of perovskite-silicon tandem solar cells was studied by subjecting the cells to similar conditions, 85°C and 85% RH, for 1000 [70] and 700 hours [74]. In these studies, the cells retained 95% [70] and 80% [74] of their initial efficiencies, respectively. In the first case, the cell was encapsulated in a sandwich architecture, with a cover glass on top and butyl rubber as an edge sealant [70]. In the second damp heat study, the cells were encapsulated using butyl rubber as an edge sealant and polyolefin elastomer (POE) as an encapsulant [74]. Herein, in addition to the damp heat test, the cell performance was measured using MPPT, under AM1.5G for 1800 hours, where the cells retained 84% of their initial efficiency [74].

Another study for PSTSCs was conducted by Hou et al., where they performed two different tests on the devices, a thermal stability test and a MPPT test [71]. To test the thermal stability, they subjected the cells under dark conditions in 85°C and 40-50% RH for 400 hours using butyl rubber as an edge sealant [71]. On MPP tracking, the TSCs were encapsulated with

polyolefin and kept under 1-Sun illumination, 40°C and 40-50% RH for 400 hours [71]. The devices had minimal losses after 400 hours in both tests [71]. A similar set of tests was performed by Al-Ashouri et al., where they studied both thermal durability and maximum power point performance [72]. Thermal durability was tested by increasing the temperature from 25°C to 85°C and then back to 25°C (200 min), which showed no loss in power conversion efficiency [72]. In MPPT, the TSCs were subjected to AM1.5G-illumination for 300 hours in 30-40% RH and the cells retained 95% of their initial power conversion efficiency [72]. In this study they used absolute photoluminescence (PL) measurements, which allowed access to both sub cells independently [72].

Outdoor aging has been performed in a few studies, one conducted by Bastiani et al. [69], and one conducted by Liu et al. [73]. In the first study, they used bifacial perovskite-silicon tandem solar cells to test the long-term performance of the devices [69]. The cells were subjected to outdoor conditions in warm and sunny conditions for a six-month period [69]. The open-circuit voltage V_{OC} and short-circuit current density J_{SC} retained their original values, while the fill factor (FF) decreased from 80% to 50% due to degradation of the perovskite layer and electrode reactions [69]. In the other outdoor condition study, the tandem cells were placed outside in warm and humid conditions (~100% RH) for 43 days, where they retained over 90% of their initial value [73]. Additionally, they performed a continuous illumination study under laboratory conditions, by MPPT the devices for over 250h under 1-Sun illumination and the devices retained their original performance [73]. In this set of studies, in addition to the continuous illumination and outdoor aging, a damp heat test was done (85% RH and 85°C) for 500 hours, where the devices maintained 87% of their efficiency [73].

Based on the literature review, long-term light soaking and maximum power point tracking (MPPT) tests are needed for perovskite-silicon tandem solar cells, as many reported studies have been conducted for durations of less than 400 hours [71], [72], [73]. Therefore, the effects of illumination on these devices still need to be studied, as tests conducted over short durations cannot reliably predict cell performance over many years of real-world conditions. Some tests still have unencapsulated devices [72], although it is an essential part to improve PSCs' stability. Thus, future studies could include light-soaking tests with a promising encapsulant in PSTSCs. Another aspect requiring further research is the effect of solar irradiation and the associated current mismatch in two-terminal (2T) tandem devices. This is more difficult to study under laboratory conditions, as solar simulators are generally limited to a fixed reference spectrum, such as air mass 1.5 global (AM1.5G). Realistically, the light absorbed by solar cells

varies depending on the location and time of the day, meaning that current matching becomes more difficult under a varying spectrum. Overall, it would be interesting to study how much of the performance loss is caused by the perovskite sub-cell alone. However, because the perovskite sub-cell is typically deposited directly on top of the silicon sub-cell, it is difficult or even impossible to measure the sub-cells separately after device fabrication, especially in 2T-cells. And, as can be seen in Table 2, no specific protocol for testing perovskite-silicon tandem cells currently exists, which complicates comparison between studies. The limited number of long-term stability studies further highlights the need for more research. Standardized protocols for testing the cells are needed, as the lack of such standards makes it difficult to compare results across different studies.

3 The Impact of Solar Spectrum Variations on Perovskite-Silicon Tandem Solar Cells

3.1 Solar Spectrum

Solar spectrum refers to the distribution of electromagnetic radiation emitted by the Sun and received at the Earth's surface, ranging from wavelengths of 300 nm to 2500 nm [75]. The spectrum includes visible, UV and infrared light [75], and it varies depending on the location and the time of the day [8]. Since photovoltaic devices are typically characterized under laboratory conditions, variations in the solar spectrum are rarely considered in studies of perovskite-silicon tandem solar cells, highlighting the need for further research in this area [76]. To allow comparison between studies, the standard reference spectra are used to ensure consistent testing for photovoltaic characterization [8]. The standard reference spectra include three different spectra: AM0, AM1.5D and AM1.5G [76]. Here, AM stands for air mass, which refers to the path length of sunlight through the atmosphere between the Sun and the receiving surface [76]. Air mass zero (AM0) refers to the solar spectrum before entering the Earth's surface, thus it is often used for space applications [76]. Air mass 1.5 directed (AM1.5D), on the other hand, means the direct sunlight coming from the Sun, often used in applications for enhancing solar cell efficiency, such as trackers or mirrors [76]. For terrestrial applications, air mass 1.5 global (AM1.5G) spectrum is the most commonly used standard [76]. It consists of both direct sunlight and light that has been scattered in the atmosphere [76]. The AM1.5G reference spectrum represents a fixed standard condition, whereas the actual solar spectrum under field conditions varies with location, weather and time [11] (Figure 7).

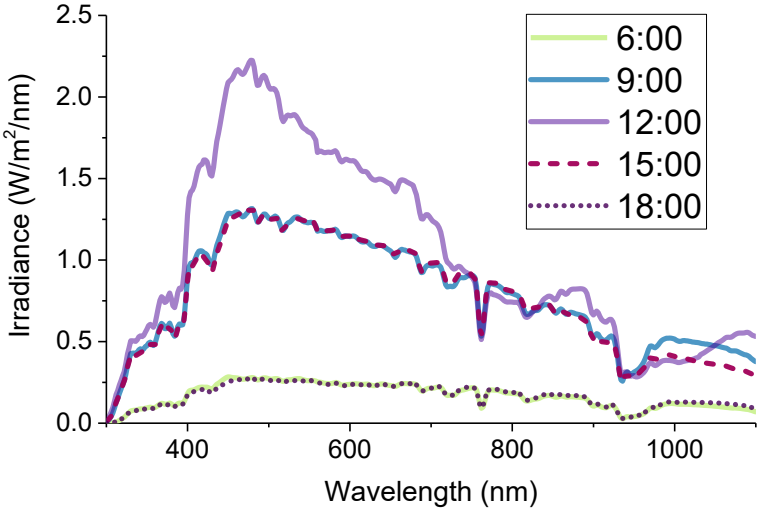

Figure 7. Solar irradiance spectrum measured at different times of day on June 1st, 2014. Data from NREL, in Golden, Colorado [77].

The AM1.5G reference spectrum used for solar cell characterization can be different from the solar spectrum, due to significant variations in light intensity and spectral distribution [11]. Several different factors can affect the solar radiation reaching the Earth's surface. When the weather is clear and the Sun is right above the surface of the Earth, around 70% of the solar radiation makes it to the Earth's surface [78]. Approximately 7% of the radiation reaching Earth's surface is diffuse light, scattered by particles in the atmosphere [78],[79]. The amount of scattered light can vary depending on weather conditions, such as air pollution or cloud coverage [78],[79]. Rest of the solar radiation is reflected or scattered back to space [78].

Therefore, sunlight reaching the Earth's surface is not constant, as it depends on fractions that are reflected, absorbed and scattered in the atmosphere. In addition to the atmospheric effects, the position of the Sun plays a crucial role in determining how much solar radiation is captured by the solar cell or panel surface [80]. Besides optimizing the tilt angle of the actual solar cell or panel, two other angles are important, which are solar zenith and azimuth angles [80]. The azimuth angle indicates the position of the Sun in the north-south direction, meaning that if the Sun is at north, the azimuth angle is zero [81]. The solar zenith angle (SZA), on the other hand, refers to the angle between the normal of the ground and the Sun [81]. Thus, if the Sun is directly overhead, SZA is 0°, and on the horizon, it is 90° [81]. Terrestrial solar irradiance is significantly affected by the solar zenith angle (SZA) [82], as it determines the amount of sunlight reaching a surface. Under clear sky and low SZA, sunlight travels through a shorter path in the atmosphere, resulting in less scattering and higher direct irradiance [83].

3.2 Effects of Solar Spectrum on Perovskite-Silicon Tandem Solar Cells

The solar spectrum variations significantly affect perovskite-silicon tandem solar cells, as the sub-cells absorb different wavelengths of the sunlight, depending on their band gap [4]. The perovskite sub-cell primarily converts light in the visible range, while the silicon sub-cell absorbs the near-infrared light that passes through the top perovskite cell [9]. Usually, the top cell has a wider band gap, and therefore it absorbs high energy photons, whereas the bottom cell has a narrower band gap and captures the low energy photons [4].

In general, the light absorbing layer should have an appropriate band gap to ensure efficient photon absorption and enable the cell to convert light into photocurrent efficiently [84]. To optimize the top cell, its band gap is tuned through compositional engineering [85], often by

modifying the composition of perovskite, for instance by substituting or mixing different cations or anions [6]. It is particularly important in two-terminal (2T) devices, which require current matching, unlike four-terminal (4T) tandems [6]. In addition to compositional engineering, temperature also affects the band gaps of the sub-cells. With increasing temperature, the band gap energy of the silicon sub-cell decreases, whereas the band gap of the perovskite sub-cell increases [86]. This is due to different lattice behaviour of silicon and perovskite materials [87]. These changes can affect the photocurrent generated by each sub-cell and therefore lead to current mismatch in the tandem device, reducing the overall performance [86].

It has been suggested that the band gap of the perovskite sub-cell could be modified according to the conditions it is operated in [6],[85]. For instance, the thickness of the light absorption layer and band gap combinations can be optimized to maximize the efficiency of perovskite-silicon tandem solar cell in different locations and temperature variations [6]. Typically, in PSTSCs the perovskite sub-cell has a band gap of 1.68 eV, which allows it to absorb light efficiently [54]. However, in outdoor conditions with varying spectra and temperature, this band gap can induce imbalances in current match and therefore cause effects such as reverse bias (RB) [54].

Current mismatch is defined as the difference between the photocurrent densities of the sub-cells:

$$CM = J_{ph,PSC} - J_{ph,Si}\,, \tag{1}$$

where CM is current mismatch, $J_{ph,PSC}$ the photocurrent density of the perovskite sub-cell, and $J_{ph,Si}$ the photocurrent density of the silicon sub-cell [11]. The cells are current matched well, when the difference between the photocurrent densities is small, ideally close to zero. Current mismatch can lead to effects such as unused photocurrent, reduced efficiency, and reverse bias, potentially leading to hot spots and accelerated degradation [11].

Reverse bias (RB) is closely linked to current matching. RB, as explained earlier, occurs in 2T tandem cells when one of the sub-cells produces less current than the other, causing the voltage across the weaker sub-cell to reverse polarity [11],[58] (Figure 8). Since the sub-cells are series connected, RB affects the performance of the entire 2T tandem device [2], and must therefore be taken into account. The sunlight reaching the cell surface can vary in outdoor conditions, as factors such as dark clouds, nearby trees or other external factors can cause partial shading of

the cells [88]. When one of the cells in a string becomes shaded, while the others remain in full sunlight, the shaded cell becomes reverse biased, which can lead to irreversible degradation and reduced current flow [11], as explained in the 2.3.3. section of this thesis.

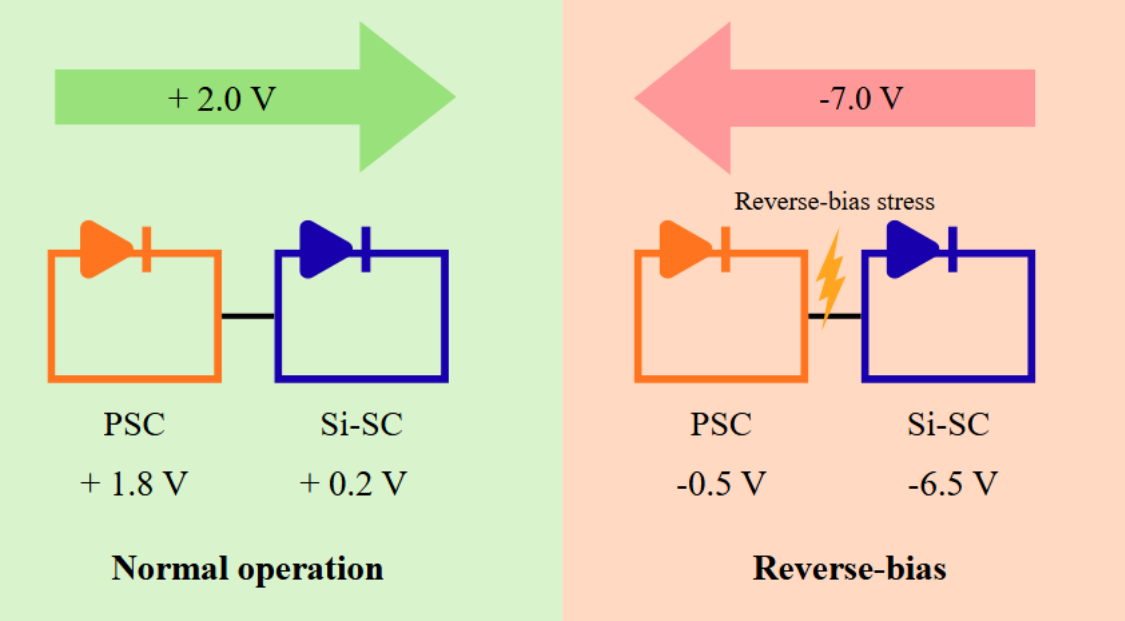

Figure 8. Comparison of normal operation of perovskite-silicon tandem solar cell (PSTSC) with reverse-bias (RB) conditions. Under RB, current mismatch forces the lower-current sub-cell into reverse-bias, resulting in high electric fields that can cause hot spots and degradation. Figure inspiration from [89].

As reverse bias occurs when the currents of the sub-cells are not matched, good current matching is one of the key factors mitigating RB effects. When both sub-cells operate at the same current, that is, they are current matched, the tandem cell becomes more resilient to RB. However, the challenge is that the sub-cells are current matched under laboratory conditions, usually under the AM1.5G spectrum, therefore they often become current mismatched under real operating conditions due to spectral variations. [11]

Previous studies, as stated in [11], have shown that cell breakdown becomes more likely under varying spectra and temperatures. Under changing illumination, the photocurrent densities vary significantly, for instance in bluer wavelength range of light the difference $J_{ph,PSC} - J_{ph,Si}$ becomes positive, and under redder wavelength range it turns negative. When the spectrum shifts from blue to red, the perovskite sub-cell can limit the current of the tandem device and may be forced into RB, potentially leading to breakdown of the perovskite sub-cell and therefore causing possible damage to the silicon sub-cell as well. Such spectral changes often occur during sunny afternoons in various locations and seasons. [11] Therefore, ensuring good current match is particularly important, as these conditions are common in real outdoor

environments. Additionally, solutions such as including more bypass diodes, reducing the number of cells in a string, or modifying the band gap of perovskite have been considered [11],[58],[88]. However, further research is needed to understand how current matching affects reverse bias breakdown in PSCs and consequently, the performance of PSTSCs.

3.3 External Quantum Efficiency

Quantum efficiency defines the ratio of collected charge carriers to incident photons and is commonly divided into internal and external quantum efficiency [90]. External quantum efficiency (EQE) includes optical losses in the device, such as reflection and transmission, whereas internal quantum efficiency (IQE) considers only photons absorbed in the active material [90],[91]. Therefore, to account the optical losses, EQE is used throughout this work to provide more accurate current generation of the tandem device.

External quantum efficiency (EQE), also known as the incident-photon-to-current conversion efficiency (IPCE), describes the wavelength dependent ratio of collected charge carriers at the electrodes, divided by the incident photons reaching the cell's surface [92],[93]. EQE is measured to study the solar cells' behaviour in a certain wavelength range [94]. It is closely related to spectral responsivity (SR), which is an important metric used to define a device's EQE [94],[95]. The spectral responsivity measurements used for determining EQE are usually conducted based on IEC 60904-8 standard [96]. Based on the standard, the measurements are conducted by illuminating the photovoltaic device and its active areas with monochromatic light, usually generated by monochromator [94]. For spectral responsivity, the short-circuit current density of the device is measured and used to calculate the spectral responsivity SR(λ) according to the following equation:

$$SR(\lambda) = \frac{I_{SC}(\lambda)}{E(\lambda)/A} = \frac{I_{SC}(\lambda)}{P(\lambda)}, \tag{2}$$

where $I_{SC}(\lambda)$ is the short-circuit current density at a specific wavelength λ, E(λ) is the irradiance of the light source at a specific wavelength λ, A is the area of the device, and P(λ) the radiant power incident on the device at a specific wavelength λ [96].

From spectral responsivity, EQE can be calculated using the following equation:

$$EQE\ (\lambda) = SR(\lambda)\frac{hc}{q\lambda}, \tag{3}$$

where SR(λ) is the spectral responsivity, h Planck's constant, c the speed of light, q the elementary charge, and λ the wavelength of the incident photons [95]. An example of external quantum efficiency of both silicon and perovskite solar cells can be found in Figure 9 for a tandem solar cell.

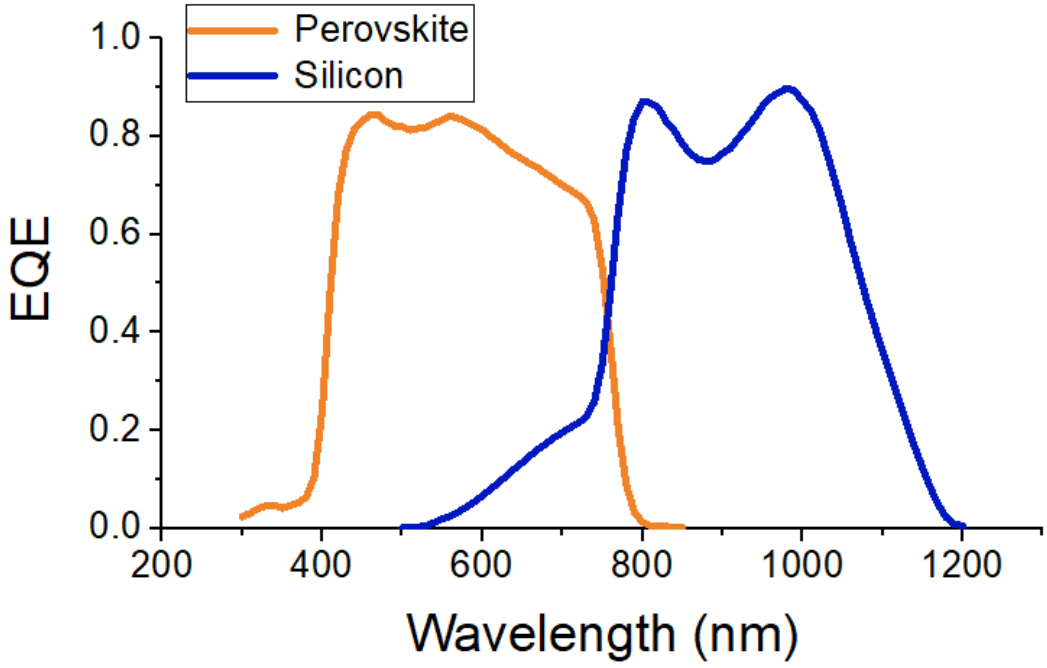

Figure 9. External quantum efficiencies for perovskite top cell (perovskite layer consisting of $Rb_{0.05}(FA_{0.83}MA_{0.17})_{0.95}Pb(I_{0.83}Br_{0.17})_3$) and silicon bottom cell (SHJ). Data retrieved from [97].

3.4 Spectral Effects and Current Matching for Perovskite-Silicon Tandems

Table 3. Overview of spectrum studies for tandem devices. The first column shows the tandem type, and the second column indicates what kind of data the studies used, followed by the methods, key findings, and other observations of the studies.

Tandem type	**Spectrum data type**	**Method**	**Spectral variation considered**	**Key findings**	**Other information**	**Ref.**
2T PSTSC modules	Outdoor measured spectral data	Theoretical + modelling	Annual variation and shading scenarios	RB breakdown is more likely under outdoor conditions, due to current mismatch	Suggested solutions to minimize RB: band gap tuning, reduced string length and MPPT	[11]
PSTSCs (2T)	AM1.5G and 20 different filtered spectra	Simulation	Calculated using a filtered spectrum	Achieved tandems with 33% PCE due to current matching and thickness optimization	Real world conditions are not considered. Ideal band gap for perovskite 1.68 eV	[57]
PSTSCs (2T)	AM1.5G- and 20 different varied spectra	Experimental	Controlled spectral variation under laboratory conditions	Experimental determination of the current-match point and its impact on device performance	PSC is the limiting sub-cell under red-rich spectra, Si-SC under blue-shifted	[98]
PSTSCs (2T and 4T)	Spectrum data from Netherlands and US, and AM1.5G	Detailed-balance calculations	Annual variation	The most affected tandem configuration is current matched 2T-device with a non-ideal bandgap	Suggested solution: location-based optimization of PSTSCs	[21]
PSTSCs (2T and 4T)	Outdoor measured spectral data	Simulation	Annual variation	Spectral deviation reduces EHE by $2\%_{rel}$	Efficiency decreases $5\%_{rel}$ with just 0.1 eV perovskite band gap change	[99]
PSTSCs (2T)	Solar simulator (AM1.5G) with varied blue content	Experimental + simulation	Controlled spectral variation under laboratory conditions	Current match significantly affects device performance, particularly FF	FF compensates for current mismatch	[100]

Not many studies for spectrum variation effects on perovskite-silicon tandem solar cells (PSTSCs) have yet been conducted. In a theoretical study by Li et al., they studied how spectral variations can affect the challenges occurring when the cells become reverse-biased [11]. To study this, they investigated how current mismatch affects the sub-cells under different spectrum and temperatures. This was done by using simulated spectral irradiance data, calculating the photon flux out of this, where the photocurrent densities (J_{ph}) could be calculated for each sub-cell. The study focused on the reverse-bias behaviour of the cells, the conditions under which these occur, and potential solutions to mitigate them. They found that PSTSCs are more susceptible to reverse-bias (RB) stress under red-rich spectra and varying temperatures. This provides a new perspective, as these conditions are not fully studied under laboratory illumination, where current matching can be achieved more easily due to optimized conditions. By considering realistic outdoor conditions with varying spectra, the study showed that achieving RB resilience in the field is significantly more challenging. Their possible solutions for this issue were a power point tracker that lets the cells operate at higher voltages, reducing cells in string, modifying perovskite sub-cells band gap and improving the RB voltage of perovskite solar cells. [11]

In this thesis, the approach used to study the current-matching behaviour of PSTSCs is fairly similar to that used by Li et al. [11], however, the focus of these two studies differs. Li et al. primarily studied the reverse-bias behaviour of PSTSCs and how environmental conditions such as temperature, albedo, and spectral variations affect the cells [11]. In contrast, this thesis focuses on determining the conditions where current mismatch occurs, identifying the limiting sub-cell, and studying how weather conditions, such as cloudiness affects the sub-cell current generation using measured spectral data under Finnish climate conditions.

In another study, Shrivastav et al. performed a simulation, where they considered the thicknesses of the light absorbing layers and the effect it has on the photon harvesting properties of the cells. In this simulation, the authors addressed current matching optically by using 20 different filtered spectra and adjusting layer thicknesses. Here, the filtered spectrum refers to the photons that pass through the perovskite top-cell after absorption, which varies with the thickness of the perovskite layer. The calculations were done by calculating the passing AM1.5G through the upper, perovskite sub-cell, and then using the transmitted photons for the bottom silicon sub-cell. This allowed a comparison of the sub-cell's photocurrents with different thickness combinations, identifying the ones that produced matched currents for the tandem device. Using this method, the authors achieved a simulated efficiency of 33% with a

tandem composed of a perovskite sub-cell (1.68 eV band gap) and a silicon sub-cell (band gap of 1.12 eV). The main limitation of this study is that it does not consider real-world conditions, such as spectral and temperature variations, which can significantly affect the results. Additionally, the study is purely simulation based and assumes ideal tunnel recombination junction (TRJ), which is the layer connecting the top and bottom sub-cells, which in practice often introduces resistive losses and therefore affect the device efficiency. [57]

Bett et al. studied spectral effects on PSTSCS, with a particular focus on current matching, using a different approach: spectrometric characterization. Instead of relying on external quantum efficiency (EQE) of both sub-cells, this method determines the short-circuit current by measuring I-V characteristics under systematically varied irradiance, ranging from blue to red-shifted spectra. This allows to determine the current match point and additionally, provide information on both sub-cells alone. According to the study, spectrometric characterization provides more reliable current matching results than EQE based approach, as it avoids measurement inaccuracies involved with sub-cell measurements in monolithic devices. In addition to providing an alternative approach for assessing current matching, the key findings of the study were that the perovskite top cell became current-limiting under red-rich spectra, while the silicon bottom cell became current-limiting under blue-shifted spectra, reflecting the spectral response of each sub-cell. [98]

Futscher et al. [21] studied the theoretical efficiency limits of perovskite-silicon TSCs, by comparing two-terminal (2T), four-terminal (4T), and module architectures and their efficiencies under two different locations: Utrecht, Netherlands, and Denver, Colorado, US. The calculations were done using detailed-balance calculations, in which the total current of each sub-cell is calculated using Shockley and Queisser [101] equations by modifying these to tandem configurations. Photocurrent of each sub-cell were calculated from the photon flux of both the standard AM1.5G spectrum and real measured solar spectra. Among the studied configurations, the current mismatch issue is most critical for two-terminal tandems, as these were found to be the most affected under varying spectra, resulting in significant power losses. In this study, Futcher et al. addresses this by modelling the effect of spectral changes on current matching in 2T-tandems, clearly stating that even if current matching is optimized under AM1.5G, real-world operation leads to significant mismatch losses. Additionally, they demonstrate that an optically thick absorber with a non-ideal band gap, such as perovskite, limits current matching by reducing the available photocurrent to the silicon bottom cell. [21]

In another study, Witteck et al. [99] studied the effects of spectral variations and band gap tuning of PSTSCs. The study was conducted by applying measured irradiance data from Golden, Colorado (US), and experimentally obtained cell parameters to model energy harvesting efficiency (EHE) of both two-terminal (2T) and four-terminal (4T) tandem devices. Energy harvesting efficiency (EHE) refers to the ratio at which a solar cell converts incident sunlight into electrical power [102]. Their main findings were that if a device is well current matched under reference spectrum (AM1.5G), in outdoor conditions and varying spectra, the EHE is only affected by $2\%_{\mathrm{ref}}$. Considering variations in the perovskite sub-cell band gap, the findings indicate that a 2T PSTSC can lose over 5% relative efficiency if the top-cell band gap deviates by 0.1 eV from the optimal value. Furthermore, they modelled with a non-optimal band gap for perovskite, which was 1.58 eV, which resulted in $17\%_{\mathrm{ref}}$ lower EHE compared to 4T device due to high current mismatch. However, while 4T devices function without current matching, in practise these devices have similar, or lower efficiencies once realistic losses, such as optical losses, are included. [99]

Köhnen et al. studied effects of spectral variation on PSTSCs and current mismatch by combining J-V measurements with short-circuit current (J_{SC}) calculations using external quantum efficiencies (EQEs) of the sub-cells. The measurements were done by using a solar simulator and varying the light composition by tuning the amount of blue light. The results showed that current mismatch does not determine the amount of power output of the cells alone, as a lower J_{SC} can be partially compensated by an increased fill factor (FF). However, FF was significantly affected by the amount of blue light in the illumination. The study also noted that varying rates of degradation can lead to increased current mismatch over time, which emphasizes the importance of improving stability, especially with PSCs. [100]

Overall, it seems that there is still a lack of studies considering spectral variability in PSTSCs, especially under real outdoor conditions. Many of the existing studies have been conducted under laboratory conditions, often using varied spectra with different wavelength compositions. However, tandem cells that are current matched under laboratory conditions may not behave similarly outdoors, as spectral and temperature variations can induce current mismatch, highlighting the importance of considering real-world conditions in future studies. Additionally, several studies only rely on simulated irradiance data and do not consider for real-world variations in spectral conditions and temperatures [11],[57]. Therefore, this thesis addresses this limitation by using real measured irradiance data that takes into account seasonal and environmental variability, including changes in cloudiness.

This thesis also addresses Finnish climate conditions, which are rarely considered in the literature. Many studies mainly focus on hot and humid environments and do not consider conditions such as cold winter days with significant cloud cover and lower illumination. Additionally, modelling studies of PSTSCs often assume an ideal recombination junction, which may lead to overestimated current generation [57]. Furthermore, many studies focus on theoretical efficiency limits [21] and therefore do not consider for degradation effects, even though degradation can significantly affect tandem device performance and current matching conditions [100]. At the time of this study, no research has yet stated how current mismatch accelerates degradation or how degradation effects current mismatch, although it has been reported that degradation can increase current mismatch [100]. However, the relationship between these effects has not been studied yet, highlighting the need for further research in this area.

A common aspect in the studies of the literature review is that the band gap of perovskite is often tuned to improve current matching conditions [21],[57], [99] and to enhance the resilience against reverse-bias conditions [11]. Additionally, it has been reported that the perovskite sub-cell often becomes the current limiting sub-cell under red spectra [11],[98]. Overall, studying the real-world operation of PSTSCs remains challenging and requires further research, as devices are still often current matched under laboratory conditions [21]. Therefore, this thesis focuses on studying the current matching conditions under real outdoor environment rather than a laboratory environment.

Based on the literature review, the most common method to assess current matching in perovskite-silicon tandem solar cells (PSTSCs) is through measuring EQE data for both sub-cells, which can then be used to determine the current mismatch. Therefore, this method was also used for the calculations in this study. While this method is commonly used for analysing PSTSCs, it has some limitations that may reduce its accuracy. This includes not taking degradation effects into account [103] and the use of EQE measurements that are typically measured under laboratory conditions at 1-Sun illumination, which introduces some uncertainty to the results [104]. Additionally, as mentioned in Section 2.3.1, ion migration can lead to changes in the perovskite layer with time, which are not fully accounted using the EQE method [104].

4 Methods

This section describes the methods behind the photocurrent density and current mismatch calculations for a perovskite-silicon tandem solar cell (PSTSC). The calculations were done in the following way: first, the irradiance measured with a spectroradiometer (MS-711) was used to determine photon flux, after which the wavelength dependent photocurrent density (J_{ph}) could be calculated for each sub-cell and the tandem cell. After this, the absolute current mismatch and relative current match could be determined and compared across different seasons.

The irradiance data, from New Energy Research Center (TUAS), were measured in Turku, Finland, using an MS-711 spectroradiometer, which recorded spectral irradiance with the wavelength range relevant for solar cells, that is from 300 nm to 1100 nm. The irradiance was measured in 5-minute intervals during 2025, from January 1st to September 12th, between 4:00 to 22:00 each day. Using a python code (Appendix 1), the irradiance was computed into photon flux, using the following equation:

$$\Phi(\lambda) = \frac{I(\lambda) * \lambda}{hc}, \tag{4}$$

where Φ is the photon flux density, I (λ) is the spectral irradiation, λ is the wavelength, h is Plank's constant and c is the speed of light [21].

After calculating the photon flux, the photocurrent densities of the sub-cells could be determined. To calculate the photocurrent density (J_{ph}) of the perovskite sub-cell, it was assumed that all photons absorbed in the perovskite layer contributes to photocurrent generation, using measured absorptance (A(λ)). Therefore, the external quantum efficiency of the perovskite sub-cell was assumed to be $EQE_{perovskite} = 1$, and the J_{ph} was calculated using the following equation:

$$J_{ph,\mathrm{PSC}} = q \int \Phi(\lambda) * A(\lambda)\, d\lambda, \tag{5}$$

where q is the elementary charge, Φ the spectral photon flux at wavelength λ, and A the absorptance of the perovskite layer at wavelength λ. For the silicon sub-cell J_{ph}, the following equation was used:

$$J_{ph,Si} = q \int \Phi(\lambda) * T(\lambda) * EQE_{Si}(\lambda) d\lambda, \quad (6)$$

where q is the elementary charge, Φ the spectral photon flux at wavelength λ, T the transmitted light through the perovskite sub-cell at wavelength λ, and EQE_{Si} the external quantum efficiency of the silicon sub-cell (SHJ). The EQE of both sub-cells is shown in Figure 10. The figure also includes the EQE of perovskite solar cell, although the EQE for perovskite was assumed to be 1 in these calculations. The absorptance and transmittance of the tandem cell were from Hägglund et al. [105], and are plotted in Figure 11. These properties correspond to a tandem cell consisting of a perovskite absorber with composition $(FACs)Pb(BrI)_3$ and a PERC silicon sub-cell [105]. Optical losses in the modelled PSTSC were simplified, as the aim of this study was to analyse current mismatch conditions, rather than absolute J_{ph} values.

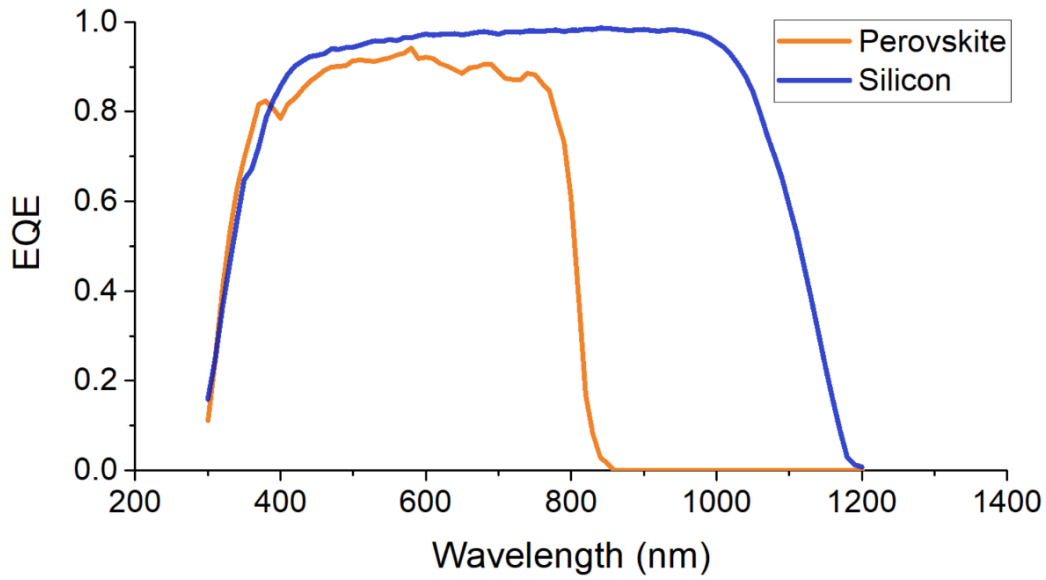

Figure 10. External quantum efficiency (EQE) of perovskite and silicon solar cells measured independently. Perovskite cell data from [106], and silicon cell data from [107]. The EQE of perovskite used here is formamidinium lead iodide ($FAPbI_3$), and the EQE of silicon heterojunction (SHJ) cell (rear-side polished). The EQE of perovskite is included in the graph for reference.

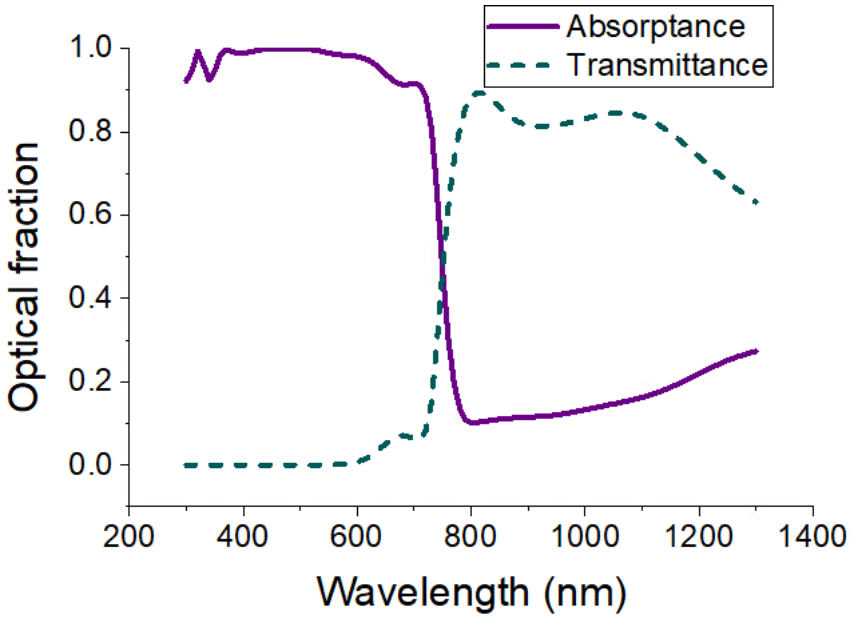

Figure 11. Modelled spectral transmittance and absorptance of the perovskite sub-cell. Perovskite structure here: $(\mathrm{FACs})\mathrm{Pb}(\mathrm{BrI})_3$. Data from [105].

The photocurrent density of the perovskite-silicon tandem solar cell was determined as the smaller of the two integrated sub-cell photocurrent densities $J_{ph,PSC}$ and $J_{ph,Si}$.

The absolute current mismatch, defined as the difference between the photocurrent densities of the sub-cells, was calculated using the following equation:

$$\mathrm{CM} = J_{ph,PSC} - J_{ph,Si}, \tag{7}$$

where $J_{ph,PSC}$ and $J_{ph,Si}$ are the integrated photocurrent densities of the sub-cells. The relative current match, which describes the balance between the sub-cell photocurrent densities, was calculated using the following equation:

$$\mathrm{CM_{rel}} = \frac{J_{ph,PSC}}{J_{ph,Si}}, \tag{8}$$

where $\mathrm{CM_{rel}}$ is the relative current match and $J_{ph,PSC}$ and $J_{ph,Si}$ the integrated photocurrent densities of the sub-cells. Seasonal weather data were obtained from the Finnish Meteorological Institute's open database [108] for Turku, Artukainen, which was the closest location with available measurements. The weather data included the cloud cover and mean temperature (°C) of each day.

5 Results and Discussion

In this chapter, the results on the current mismatch behaviour of perovskite-silicon tandem solar cells (PSTSCs) are studied under different seasons and times of the day. First, the temporal behaviour of the sub-cells and the tandem are discussed, with the focus on individual days and the effect of irradiance on photocurrent densities of the cells. This section is followed by the analysis of the effects of cloudiness and seasonal variations on current matching. Finally, the trends across all seasons are studied to identify the key patterns in PSTSC performance under varying environmental conditions.

5.1 Daily Variation of Current Match

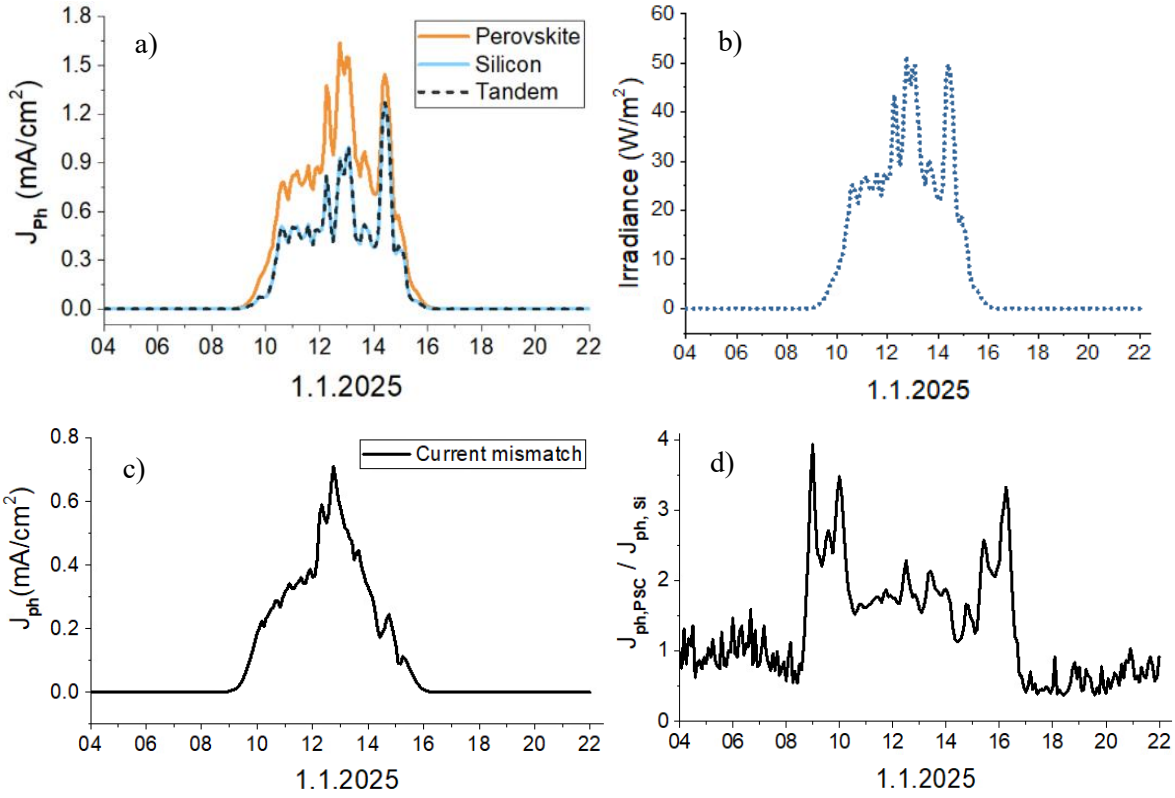

Figure 12. Figures from a cloudy winter day. A) Photocurrent density (J_{ph}) of both sub-cells (perovskite in orange and silicon in blue), and as a tandem device. B) Irradiance as a function of time. C) Absolute current mismatch of the perovskite-silicon tandem solar cell (PSTSC). D) Relative current match of the PSTSC.

On a cloudy winter day, when the temperature is around -5°C, the irradiance remains relatively low throughout the day (Figure 12B), resulting in low photocurrent densities (J_{ph}) in both sub-cells (Figure 12A). Because the cells are series connected, the sub-cell generating the lower current limits the total tandem current. In this case, the silicon sub-cell produces the lower current, and therefore determines the overall device current (Figure 12A). The J_{ph} curve of

perovskite closely follows the structure of the irradiance curve, reflecting its strong absorption in the visible light region of the solar spectrum (Figure 12A).

As the current stays low, (below 1.5 mA/cm²), the current mismatch stays below 0.8 mA/cm² (Figure 12C). The J_{ph} reaches its maximum around midday, as might be expected due to the peak in the irradiance. However, when looking at the relative current mismatch of the perovskite-silicon tandem cell, it seems that the ratio between $J_{ph(PSC)}/J_{ph(Si)}$ reaches its peak in the morning and in the afternoon (Figure 12D). At these times, the solar spectrum is more red shifted, meaning that the perovskite sub-cell is more affected due to its higher band gap, since fewer photons have sufficient energy to be absorbed by the perovskite sub-cell. In contrast, the silicon sub-cell benefits from the increased proportion of red-shifted light. Overall, the peaks in the J_{ph} ratio may be partly due to low photocurrents values, where small fluctuations can lead to large variations in the ratio.

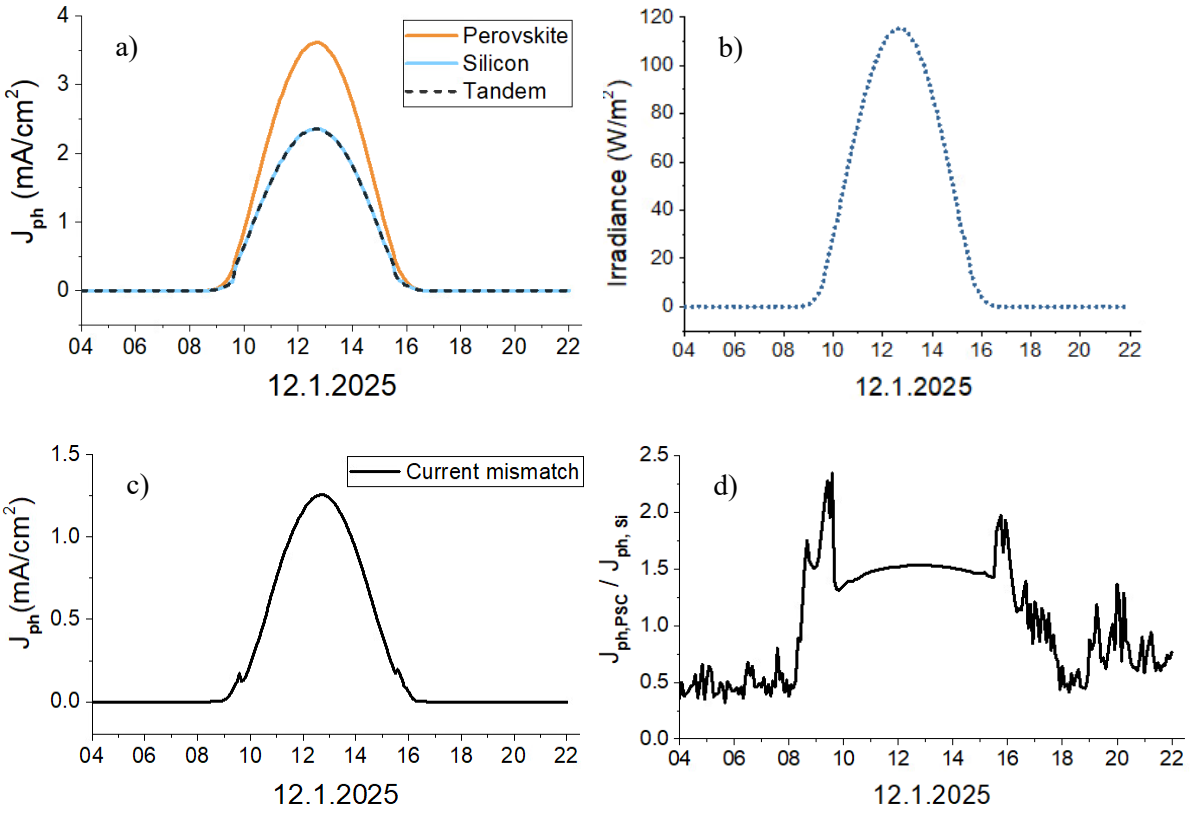

Figure 13. Graphs from a clear winter day. A) Photocurrent density (J_{ph}) of both sub-cells and as a tandem device. B) Irradiance on a clear winter day. C) Current mismatch of the perovskite-silicon tandem. D) Relative current match of the device.

On a clear winter day in January, when the temperature is around -7°C, the photocurrent density J_{ph} does not exceed 4 mA/cm² (Figure 13A), which is consistent with the low irradiance below 120 W/m² (Figure 13B) throughout the day. Again, the J_{ph} of perovskite

sub-cell follows the structure of the irradiance curve, as it is assumed to be strongly absorbing in the visible light range. The irradiance on a clear winter day reaches its maximum around noon (Figure 13B) and does not show significant variation throughout the day. A similar trend can be observed for the absolute current mismatch, which peaks around the same time as the irradiance and photocurrent densities, showing little to no variation outside its maximum (Figure 13C). In contrast, the relative current matching ratio varies more during the morning and late afternoon, showing noticeable variations in these periods (Figure 13D). The variation in relative current matching reflects the effect of spectral changes during a winter day with a clear sky but can also be due to the low photocurrents during winter days, as mentioned in the case of the cloudy winter day.

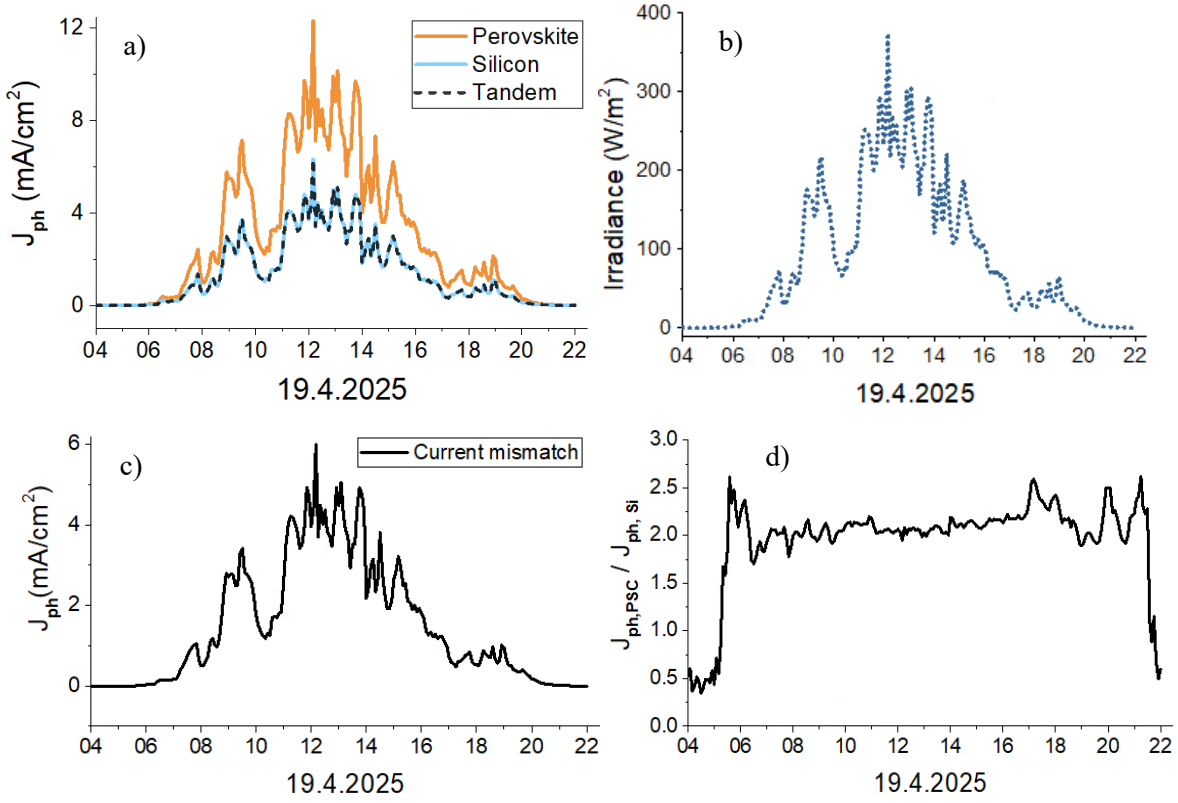

Figure 14. Graphs from a cloudy spring day. A) Photocurrent density (J_{ph}) of the sub-cells and as a tandem. B) Irradiance of a cloudy spring day as a function of time. C) Current mismatch of the tandem device. D) Relative current mismatch of the PSTSC.

During a cloudy spring day in April, when the temperature is around 13°C, the irradiance shows strong variability with multiple peaks and dips (Figure 14B). A similar behaviour is seen for the photocurrent densities of the sub-cells (Figure 14A). The silicon sub-cell remains as the limiting sub-cell, meaning the series connected tandem's J_{ph} stays at the level of the silicon cell.

When comparing the current mismatch of this cloudy spring day to the cloudy winter day, the J_{ph} of the cells is higher, with the current mismatch following this trend (Figure 12C and Figure 14C). As expected, the absolute current mismatch increases when the sub-cells, and therefore the tandem cell, produce higher photocurrent densities. With the varying irradiance (Figure 14B), the current mismatch of the tandem cell varies more than with a clear curve (Figure 12C). Additionally, the ratio of the J_{ph} of the perovskite and silicon sub-cells (Figure 14D) does not show peaks in the morning and late afternoon, as with those observed during the winter days. This might also be due to higher absolute photocurrent densities, for which the J_{ph} ratio becomes less sensitive to fluctuations. Overall, during cloudy spring conditions, the perovskite sub-cell remains as the dominant sub-cell, likely due to enhanced diffuse light caused by clouds or the amount of blue-rich sunlight.

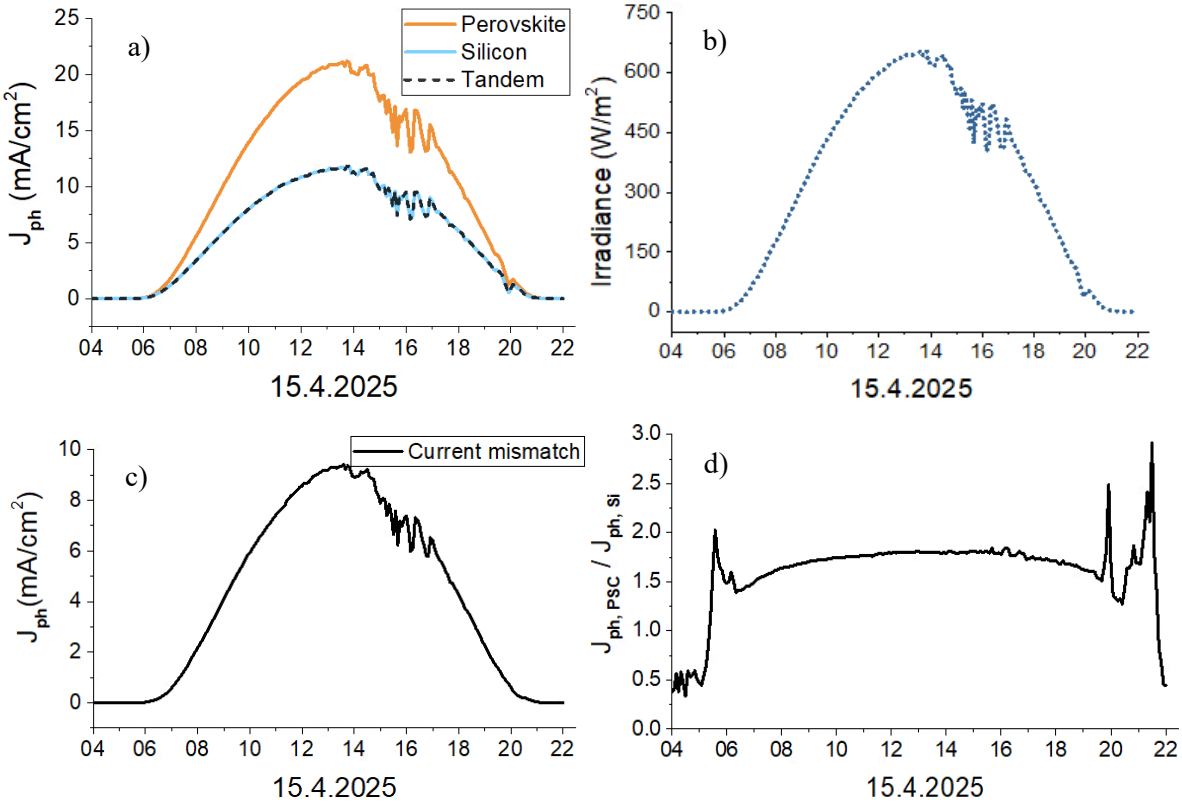

Figure 15. Graphs from a clear spring day. A) Photocurrent density (J_{ph}) of the tandem device and the sub-cells (in orange PSC, in blue Si-SC). B) Irradiance on a clear spring day. C) Current mismatch of the tandem cell. D) Relative current mismatch of the tandem.

A clear spring day shows a higher irradiance (Figure 15B) and therefore higher photocurrent densities (J_{ph}) (Figure 15A) compared to a cloudier day (Figure 14B). Again, the silicon cell remains as the limiting sub-cell, limiting the J_{ph} of the whole tandem cell (Figure 15A). Here, both the irradiance and photocurrent densities reach their maximum around noon, with relatively small variations throughout the day, except some fluctuation in the late afternoon.

The current mismatch follows the same trend as with J_{ph} and irradiance, showing its peak value around 10 mA/cm² in noon (Figure 15C). Regarding the relative current mismatch, the J_{ph} ratio remains relatively stable throughout most of the day, with two peaks observed in the early morning and late evening. The cloudy spring day (Figures 14A-D), show more fluctuations in irradiance, photocurrent densities and current mismatch compared to this clear spring day, which may be because of the cloudy conditions and therefore more diffused sunlight.

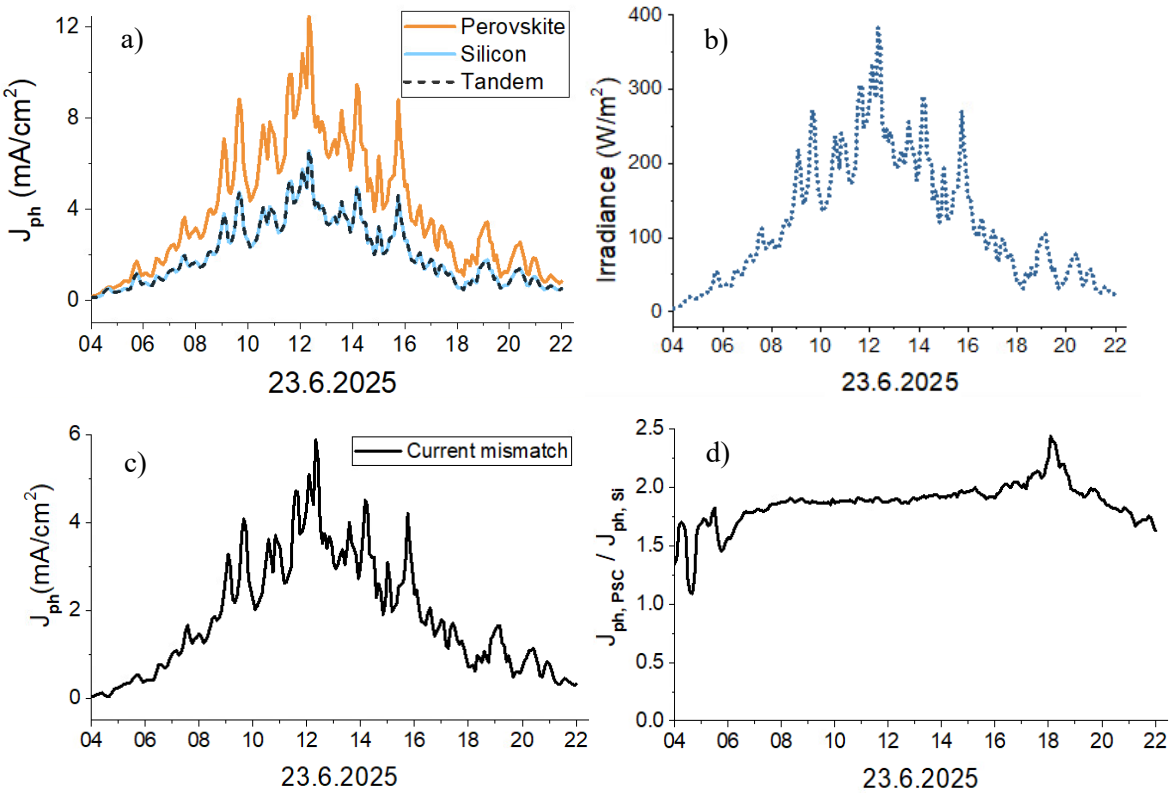

Figure 16. Graphs from a cloudy summer day. A) Photocurrent density (J_{ph}) of the sub-cells and PSTSC. B) Irradiance on a cloudy summer day. C) Current mismatch of the PSTSC. D) Relative current mismatch of the PSTSC.

On a cloudy summer day, with a temperature of around 14°C, the irradiance shows strong variability (Figure 16B), even though the Sun stays above the horizon for most of the time during this time due to Finland's high latitude. Most likely strong cloud cover causes the fluctuation, limiting the irradiance and therefore causing high variability in the photocurrent densities (J_{ph}) of the cells as well (Figure 16A). Again, the J_{ph} of the tandem cell is limited by the lower current producing silicon sub-cell (Figure 16A).

The absolute current match also shows high variations, with its peak reaching around 6 mA/cm² around midday (Figure 16C). The ratio of $J_{ph(PSC)}/J_{ph(Si)}$ stays relatively stable and reaching its maximum value during the afternoon (around 18:30), indicating a temporary increase in

current mismatch between the sub-cells (Figure 16D). The peak could be due to changes in spectral conditions, such as the cloudiness, causing a temporary increase in the J_{ph} of the perovskite sub-cell. Overall, the perovskite sub-cell is dominant throughout the day, however, at certain times (such as around 6:00 in the morning) the ratio approaches 1, indicating nearly equal photocurrent generation in both sub-cells.

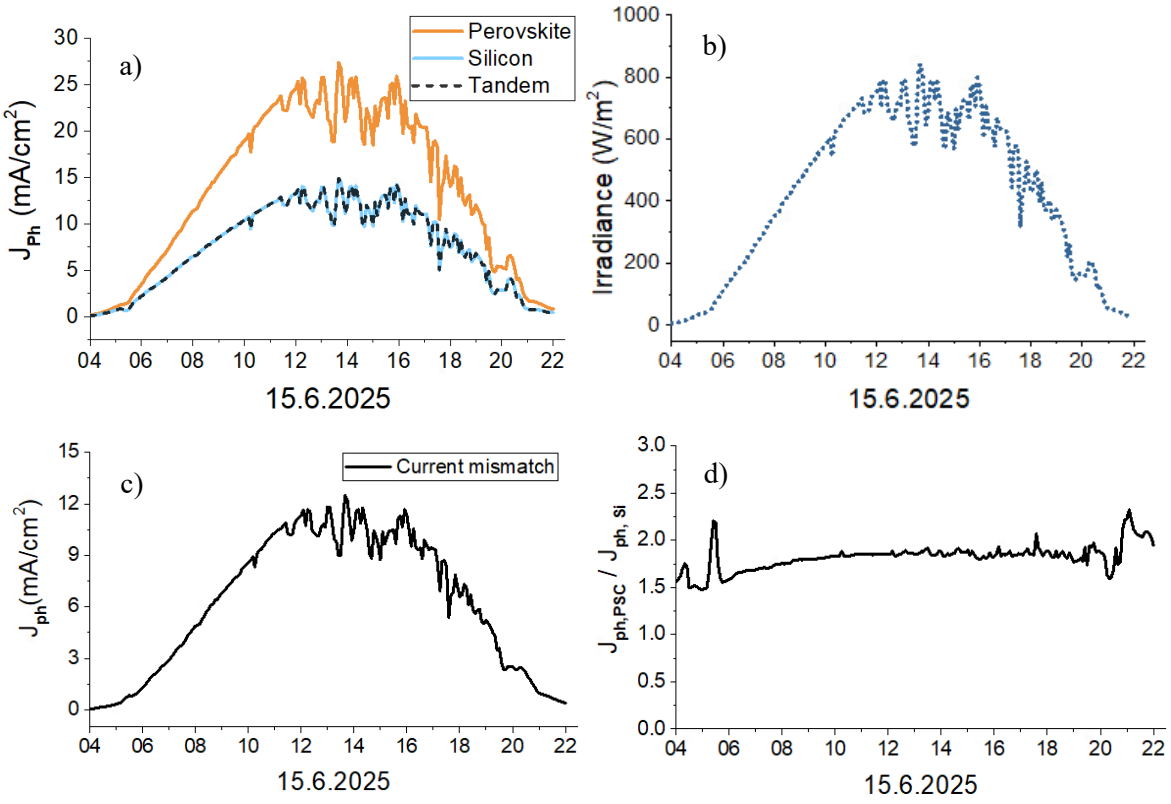

Figure 17. Graphs on a clear summer day. A) Photocurrent density (J_{ph}) of the sub-cells and the tandem as a function of time. B) Irradiance on a clear summer day. C) Current mismatch of the perovskite-silicon tandem. D) Relative current mismatch of the tandem.

On a clear summer day during the Finnish mid-summer (~20°C), the irradiance is fairly high (Figure 17B), meaning that the photocurrent densities also reach higher values (Figure 17B). There is less variation in the morning in all three graphs (J_{ph} (Figure 17A), irradiance (Figure 17B), and current mismatch (Figure 17C)), with the variability increasing after midday. This can be due to changing weather conditions such as clouds passing by the measurement location.

Overall, during this day, the current mismatch is the largest out of the seasons discussed so far, reaching more than 12 mA/cm² (Figure 17C), likely due to increased irradiance. However, the relative current mismatch (Figure 17D) is comparable to that observed on the cloudy summer day (Figure 16D). The ratio remains stable, with values around 1.75, but shows peaks in the early morning and late evening, following a similar trend observed during the cloudy day.

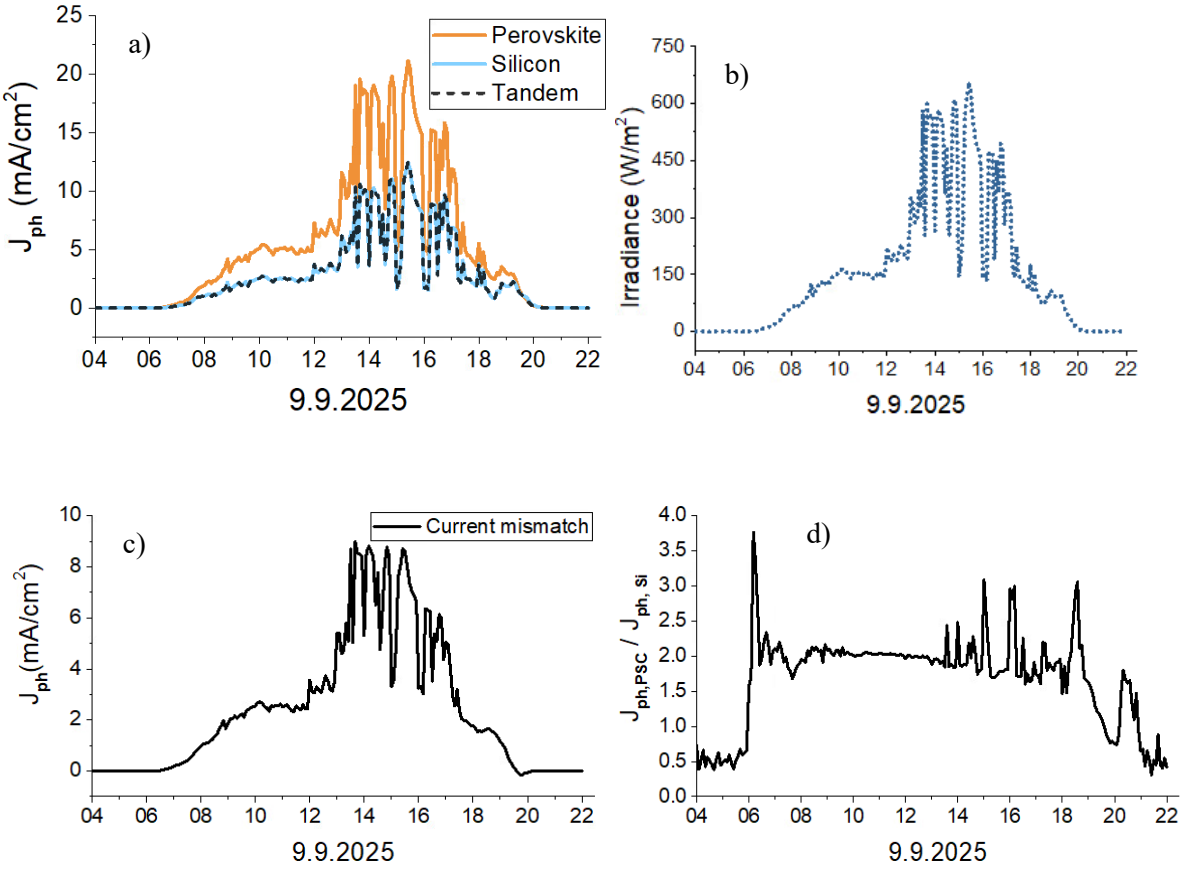

Figure 18. Graphs from a cloudy autumn day. A) Photocurrent density (J_{ph}) of the tandem and the sub-cells (perovskite and silicon). B) Irradiance on a cloudy autumn day. C) Current mismatch of the tandem cell. D) Relative mismatch as a function of time.

Even under cloudy conditions, the autumn day shows comparatively high irradiance (Figure 18B), resulting in higher photocurrent densities (J_{ph}) for both sub-cells (Figure 18A). The J_{ph} of the tandem remains limited by the silicon sub-cell (Figure 18A). The cloudy conditions result in high fluctuating J_{ph} in both sub-cells, which can be seen in the absolute current mismatch as well (Figure 18C). Current mismatch reaches up to 9 mA/cm², especially in the afternoon, indicating a significant imbalance between the photocurrents of the two sub-cells. The same phenomenon can be observed for the relative current mismatch (Figure 18D), which reaches maximum values in the early morning and afternoon, indicating that the perovskite sub-cell dominates the photocurrent generation during these times. This may be due to the cloudy conditions, which can scatter the light and enhance its proportion of blue-rich light.

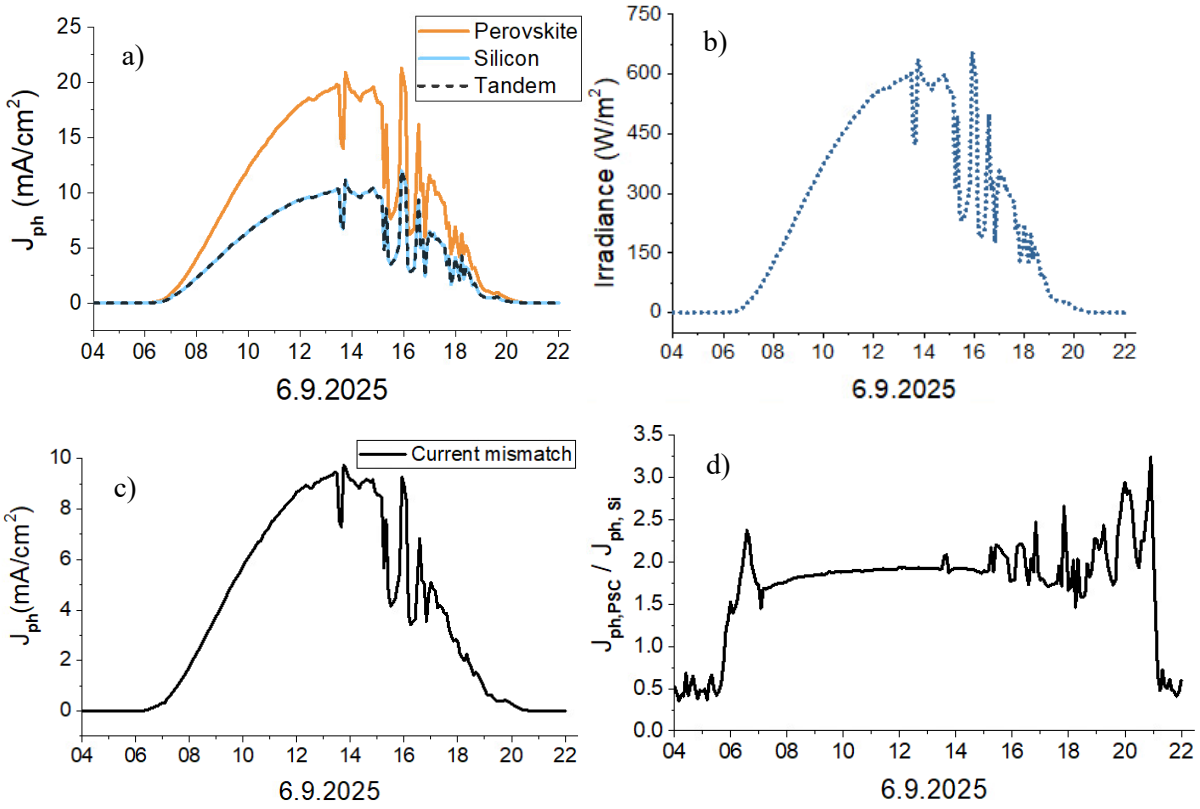

Figure 19. Graphs from a clear autumn day. A) Photocurrent density (J_{ph}) of the sub-cells and the tandem cell. B) Irradiance on a clear autumn day. C) Current mismatch of the tandem cell. D) Relative current mismatch on a clear autumn day.

Both the irradiance (Figure 19B) and the photocurrent densities (Figure 19A) exhibit increased variability during the afternoon on a clear autumn day. As this day is in early autumn in September, comparatively high irradiance levels are still observed (Figure 19B). The current mismatch between the two sub-cells remains high (Figure 19C), with larger values than those observed on the cloudier day (Figure 18C). Again, a similar trend in the absolute current match values can be seen in Figure 19D, where the ratio of J_{ph} reaches its maximum values around the early morning and evening.

5.2 Effect of Cloudiness on Current Mismatch

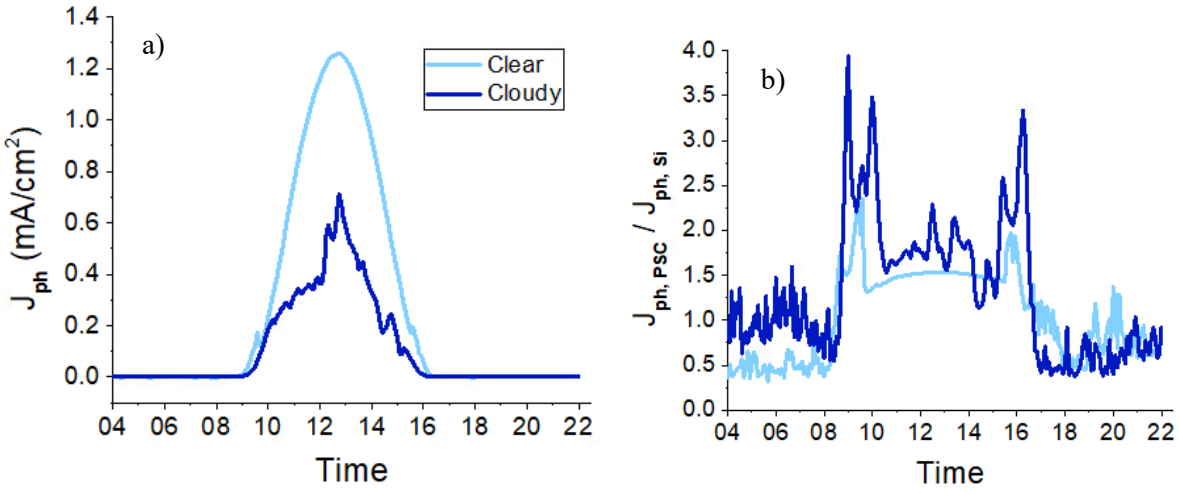

Figure 20. A) Absolute current mismatch comparison of a cloudy and a clear winter day. B) Relative current match on a cloudy and a clear winter day.

The absolute current mismatch between the perovskite and silicon sub-cells on a clear and a cloudy winter day shows a clear difference between the days (Figure 20A). On a clear day, the current mismatch reaches higher values, most likely because the photocurrent density is also higher at that time. However, on both days the mismatch does not reach high values, staying below 1.4 mA/cm² (Figure 20A). Ideally, the current mismatch would be close to zero. In this case, these kinds of conditions can be observed during the mornings and evenings on both cloudy and clear days but may also be due to the lack of sunlight in Finland on such winter days.

The ideal relative current mismatch ratio is near one, as then the sub-cells produce nearly the same amount of J_{ph}, meaning the current mismatch is close to zero, which is ideal for tandem operation. In Figure 20B during the early morning and late evening, the J_{ph} ratio is even under one, which would indicate that the silicon sub-cell is producing more J_{ph} during those times. This is because the spectrum is red-shifted in the morning and late evening, which benefits the silicon sub-cell, as they are able to absorb lower-energy photons more effectively. Apart from the mornings and evenings, the ratio of the photocurrent densities peaks up to 4, meaning that the perovskite sub-cell produces significantly more current on those times, at least on the cloudier day (Figure 20B). Overall, during winter in Finland, low irradiance leads to low absolute J_{ph} values, making the relative current mismatch more sensitive to small variations. As a result, peaks in the J_{ph} ratio more noticeable, even though the absolute photocurrents remain low.

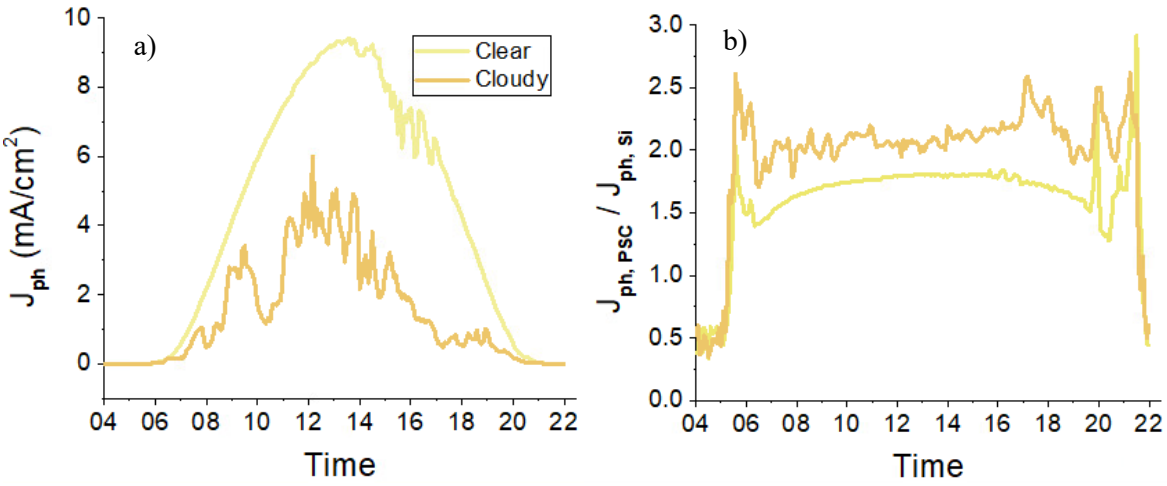

Figure 21. A) Absolute current mismatch of a PSTSC on a clear and cloudy spring day. B) The relative current mismatch of the PSTSC on both clear and cloudy day in spring.

On both spring days, i.e., cloudy and clear, the current mismatch is noticeable, as can be seen in Figure 21A. The cloudy day shows more variation in the mismatch during the day, while the clear day shows high values of around 9 mA/cm² during the day but less variability in the values (Figure 21A). The increased variation under cloudy conditions may be due to fluctuations in irradiance caused by clouds, which causes the sub-cells to respond differently because of their different band gaps, showing more fluctuation both in the actual J_{ph} values and J_{ph} ratios. The mismatch is already significantly higher than with the winter days (Figure 20 A) during both spring days. The relative current mismatch, that is the ratio of the J_{ph} of the sub-cells shows clear peaks in the early morning and late evenings on both days (Figure 21B). Surprisingly, the J_{ph} ratio remains lower on the clearer day as with in the cloudier day, indicating that the J_{ph} production of the cells is more in balance during the day when the weather is clearer. However, on both days, the perovskite sub-cell seems to produce significantly more photocurrent, which may also be partly due to the simplified optical losses in these calculations being lower than in reality, overestimating the J_{ph} of the perovskite sub-cell.

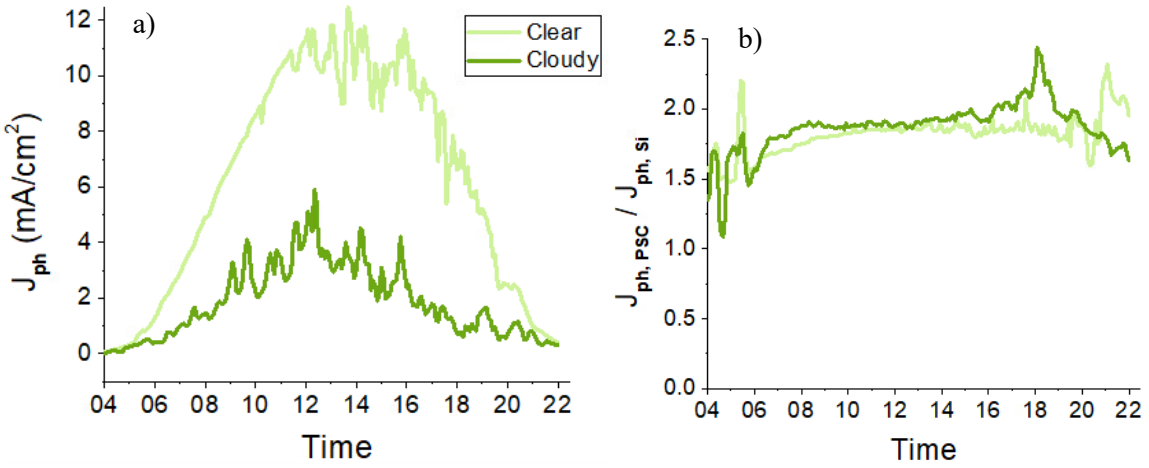

Figure 22. A) Current mismatch comparison of a clear and cloudy summer day in June. B) The relative current mismatch on the same days.

In Finland, midsummer is the time when there is the most daylight, which is also reflected in the tandem J_{ph} output and increased current mismatch (Figure 22A). The difference between a cloudy June day and a clearer, sunnier day is significant. During the clear summer day, the current mismatch reaches values up to 12 mA/cm², while on the cloudier day the values remain below 6 mA/cm² (Figure 22A). However, when comparing the ratio between the photocurrent densities of the sub-cells, it seems that those differences are not that noticeable between the two days (Figure 22B). Both ratios of J_{ph}s, remain quite stable around 2, meaning that the perovskite sub-cell produces a lot more current when comparing it to the limiting silicon sub-cell.

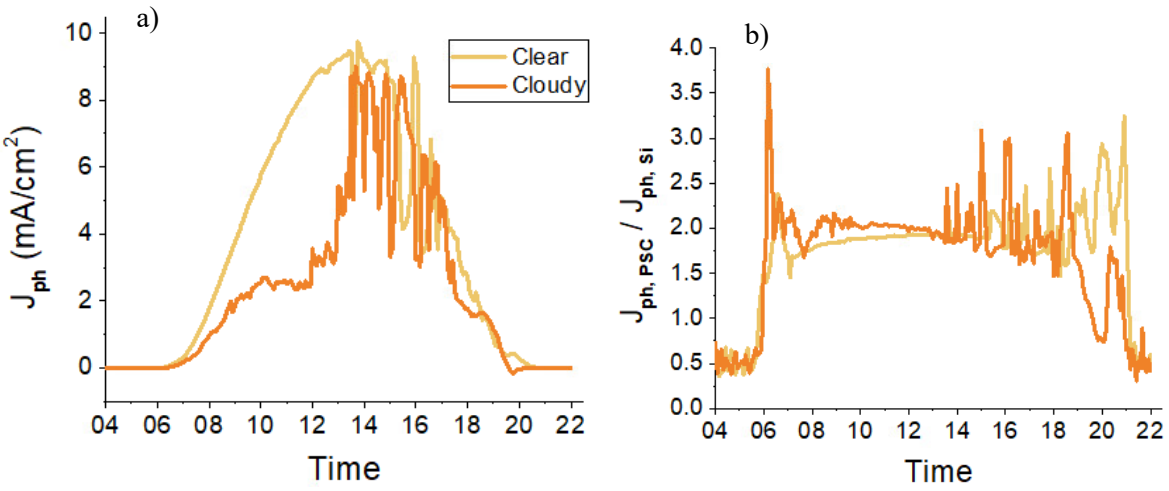

Figure 23.A) Current mismatch of the tandem cell on a clear and sunny day in autumn. B) Relative current mismatch on a clear and sunny day.

During the autumn days, the current mismatch is high, as it reaches values of up to 10 mA/cm² on both days (Figure 23A). On the clear day, the curve is relatively smooth, whereas on the cloudy day it shows lower values in the morning and a lot of variation in the afternoon, as can

be seen in Figure 23A. The ratio of the photocurrent densities J_{ph} (Figure 23B), exhibits smaller deviations than the absolute photocurrent densities. Higher J_{ph} ratios are observed during the early morning on the cloudy day, indicating increased current imbalance, while during the afternoon both days show increased variability in the ratio (Figure 23B). Overall, the J_{ph} ratio does not remain close to the ideal matching condition close to one, suggesting that optimal current matching is rarely achieved.

In summary, the perovskite sub-cell generally dominates the photocurrent generation in the tandem device during the compared times. The silicon sub-cell shows peaks in photocurrent generation during early mornings and late evenings, especially under low irradiance conditions. This is likely due to the red-shifted spectrum at these times, which is more favourable for the silicon sub-cell. Peaks in the J_{ph} ratio are typically more significant on cloudy days, which can be due to fluctuations in the irradiance and incoming sunlight, which affects the cells differently. In addition, in these calculations, the model assumes simplified optical losses for the perovskite sub-cell, which leads to an overestimation of its photocurrent generation compared to the silicon sub-cell. The mismatch is high under most conditions, which can be partly due to the assumption that the perovskite sub-cell absorbs all photons. Including more realistic optical losses would likely reduce the mismatch and provide more accurate results.

5.3 Seasonal Variation in Current Mismatch

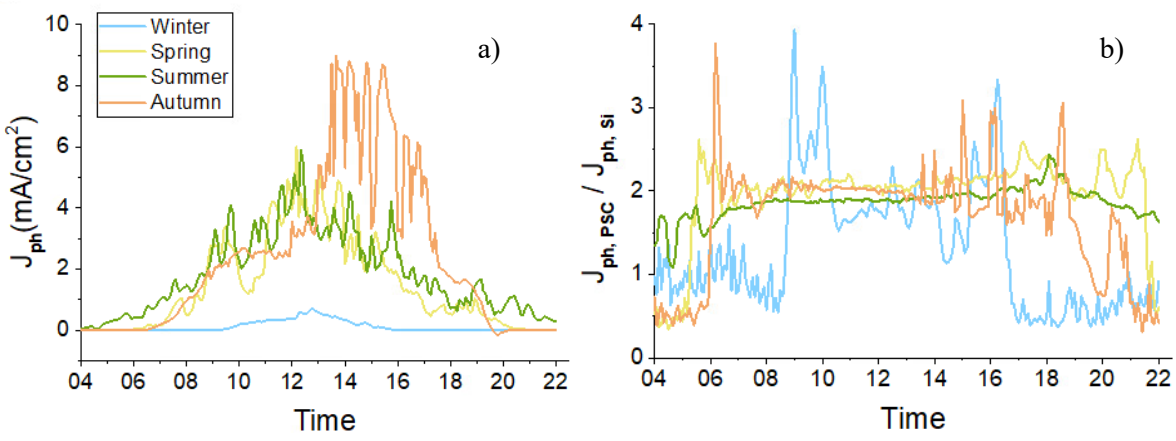

Figure 24. A) Comparison of absolute current mismatch values on cloudy days during the winter, spring, summer, and autumn for a perovskite-silicon tandem solar cell. B) Relative current mismatch during cloudy days in different seasons.

Figure 24A presents the absolute current mismatch on cloudy days across all four seasons for a perovskite-silicon tandem solar cell. The mismatch reaches its highest values during the autumn afternoon, indicating high imbalance between the sub-cell photocurrent generation. The cloudy

days in spring and summer show comparable mismatch values, whereas the winter day shows significantly lower values throughout the day (Figure 24A), which can be connected to the generally low irradiance levels during winter in Finland. However, if irradiance alone was the dominant factor, the summer day would be expected to show the highest J_{ph}, and corresponding mismatch values, given the higher solar irradiance typical of Finnish summers. This is not observed for the cloudy summer day, indicating that additional factors, such as cloudiness and variability play a significant role. Overall, the current mismatch varies a lot across all seasons, with the winter day showing less variation compared to the other seasons (Figure 24A).

The relative current match for the cloudy days can be seen in Figure 24B. The ratio of the photocurrent densities exhibits significant variability across all seasons under cloudy conditions, which may be due to clouds scattering the incoming light. During the cloudy winter day, the J_{ph} ratio approaches value close to one in the morning and late evening, fluctuating around this value and indicating that the sub-cell current are most closely matched during these times (Figure 24B). The J_{ph} ratio shows some peaks during the late morning and early evening hours. The cloudy winter day shows the most distinct curve compared to the other seasons, which may be due to low absolute J_{ph} values. As a result, fluctuations appear more high, even though the overall photocurrents remain low. In contrast, other seasons, e.g. spring, summer, and autumn, have more similar photocurrent density ratios, with higher values in the morning and evening and a relatively stable ratio around midday (Figure 24B). These peaks indicate that the perovskite sub-cell is the more dominant sub-cell compared to the silicon sub-cell during these periods. Overall, the high amount variability in both absolute and relative current mismatch can be due to cloudy conditions, which leads to scattered incoming light. In addition, the simplified optical losses overestimate perovskite sub-cell photocurrent generation and likely underestimate silicon sub-cell photocurrent generation.

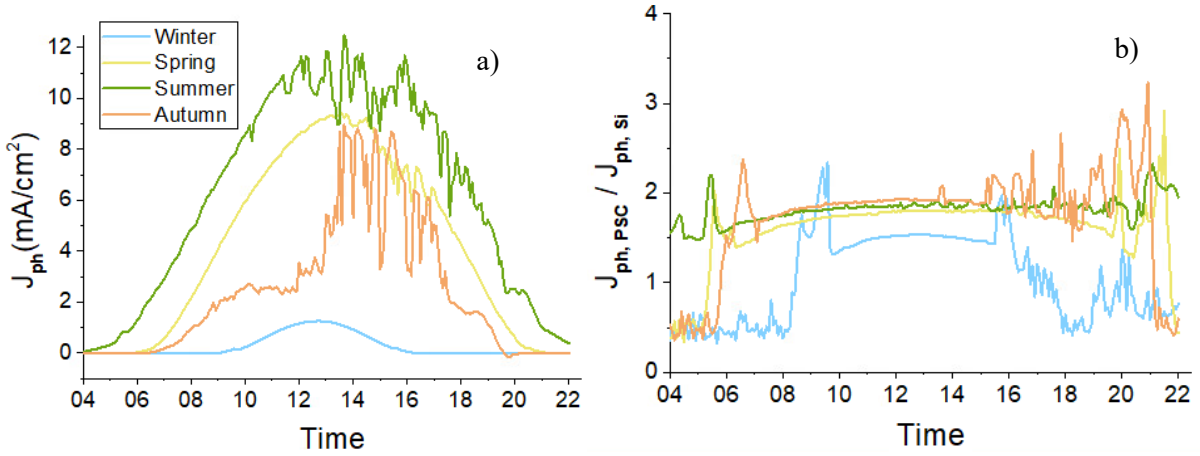

Figure 25. A) Comparison of current mismatch values on clear days across all seasons for perovskite-silicon tandem solar cell (PSTSC). B) Relative current mismatch during clear days in different seasons.

Figure 25A shows the absolute current mismatch on clear days across all seasons for a PSTSC. The mismatch values vary considerably between the seasons. The winter day exhibits the lowest mismatch throughout the day, likely due to the generally low irradiance in Finland during winter, even under clear conditions. On the clear autumn day, the mismatch increases after midday, showing a lot of variation in the absolute values (Figure 25A). This may be due to the oversimplified optical losses, underestimating silicon sub-cell photocurrent generation. Additionally, decreasing irradiance during autumn afternoon may enhance the sensitivity of the photocurrent values, leading to fluctuations in the absolute values. The spring day reaches values of around 9 mA/cm², following the daylight pattern, with a peak around noon, which may be due to increased irradiance during that time. The summer day reaches the highest mismatch of all seasons and shows significant variation throughout most of the day, except during the early morning. The mismatch does not reach zero at any time during daylight hours, reflecting the high irradiance typical of Finnish summers, particularly in June.

Figure 25B presents the relative current matching of the PSTSC. The photocurrent density ratio is similar for the spring, summer and autumn days, between approximately 10:00 and 16:00. Outside this time window, greater variations can be seen, with the autumn day showing the largest variation during the late afternoon (after 16:00). Overall, the ratio $J_{ph(PSC)}/J_{ph(Si)}$ remains below 2 during these periods, which indicates that the operation of the tandem cell is mainly limited by silicon sub-cell. These results are likely to differ if optical losses were considered more accurately, since the J_{ph} of the silicon sub-cell is likely lower than in reality. The clear winter day differs the most from the other seasons, showing constantly lower J_{ph} ratio values, and only a few peaks in the morning and afternoon, occurring at similar times as

observed for the cloudy winter day (Figure 24B). However, there are some fluctuations on the winter day a swell, which is likely due to the small irradiation and therefore also low absolute J_{ph} values and high fluctuations of relative current mismatch values.

To summarize the results, it was observed that increasing irradiance on a daily timescale led to higher absolute current mismatch. The perovskite sub-cell closely follows the temporal structure of the irradiance, which reflects its strong response to the visible part of the solar spectrum and its contribution to photocurrent generation in that spectral range. Cloudy days exhibited more variability in current matching across all four seasons, whereas clear days showed smoother curves and more structured daily trends. Some variation was observed on clear days as well, especially during the afternoon. In summary, cloudy conditions led to higher variability in the absolute current mismatch, which may be due to clouds scattering the incoming sunlight.

For the relative current match, which indicates how well the sub-cells in the tandem cell are balanced, the ratio of the photocurrent densities led to higher values around midday, likely due to increased irradiance. Higher variability in the J_{ph} ratio of the sub-cells was observed during the mornings and evening hours, which can be due to spectral changes, such as red- or blue-shifted spectra. It was observed that, for instance on a cloudy summer day, the season alone did not determine high current mismatch, as relatively low mismatch values were obtained that day. This indicates the weather conditions have a strong impact on current mismatch.

Table 4. Comparison of absolute current mismatch values during the measurement period (January-September).

Season	Average current mismatch (mA/cm²)	Overall average current mismatch (mA/cm²)
Winter	0.36	2.81
Spring	2.89	
Summer	4.62	
Autumn	2.76	

When comparing the absolute current mismatch values across seasons (Table 4), it can be seen that lower irradiance leads to lower average mismatch values. For instance, during the winter months of the measurement period (January-February), when irradiance is low, the average values of current mismatch are also low, with an average value of 0.36 mA/cm² (Table 4). During spring (March-May) and autumn (from mid-August to mid-September), when the irradiance is lower than during summer, the average values of current mismatch reach similar values of around 2.76 to 2.89 mA/cm². During the summer months (June to mid-August), the mismatch reaches its highest average values, likely due to higher irradiance in Finland during this period. For the whole measurement period (January to mid-September) the current mismatch is on average around 2.81 mA/cm² (Table 4), which means that on average, the perovskite sub-cell is producing more current when comparing it to the silicon sub-cell under these conditions. This may be explained by the simplified optical losses of the perovskite sub-cell, assuming that all absorbed photons are used in photocurrent generation.

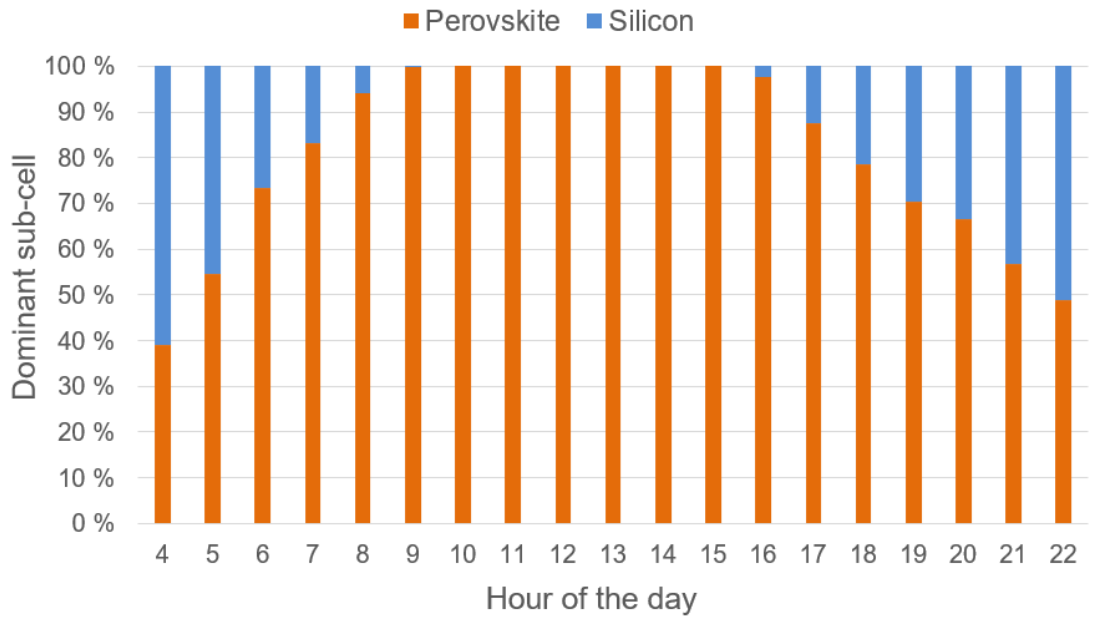

Figure 26. Hourly comparison of perovskite and silicon sub-cells producing higher photocurrent densities (J_{ph}) during the measurement period (January-September).

To further analyse which sub-cell produced higher photocurrent density during the measurement period, Figure 26 shows the hourly comparison between the perovskite and silicon sub-cells from January to September. The perovskite sub-cell is mostly producing more J_{ph} compared to the silicon sub-cell, particularly during the midday, when the irradiance is highest and the spectrum is blue shifted (Figure 26). This is likely due to the higher band gap of perovskite, which enables more efficient absorption of high energy photons in blue-rich spectra. In contrast, the silicon sub-cell produces more J_{ph} during early morning and late

evening (Figure 26) due to its lower band gap, which allows it to absorb a larger fraction of the red-rich spectrum compared to the perovskite sub-cell. However, as mentioned previously, the photocurrent density of perovskite sub-cell is most likely overestimated, as the optical losses in this model assume that all absorbed photons in the perovskite sub-cell are producing J_{ph}. Under more realistic conditions, the silicon sub-cell could produce more J_{ph}, especially in the mornings and evenings, when the spectrum is red shifted. Here, the silicon sub-cell produces slightly higher J_{ph} on average during early morning and late evening, but only for a limited time. This is expected based on the spectral response of the sub-cells and their band gaps.

Overall, the silicon sub-cell was the limiting sub-cell under most conditions, which may partly be due to simplified assumptions used in these calculations. It was also observed that on average the perovskite sub-cell contributed more strongly to current production during the evening and morning hours, which can be due to spectral changes occurring at low solar elevations. It seemed that ideal current match is rarely achieved, and only observed under low irradiance conditions, such as during a cloudy winter day, indicating that more research and detailed modelling are needed to fully understand the factors affecting the current mismatch. Additionally, these findings highlight that current matching in PSTSCs is strongly affected by spectral and atmospheric conditions and is important to consider when designing these types of cells. In this study, due to the lack of available data, the band gaps and other properties of the perovskite-silicon tandem solar cells were not adapted to the specific location, although such optimization could improve their suitability for Finnish climate conditions.

5.4 Accuracy of Results

The accuracy of the results presented in this thesis are discussed by evaluating the main modelling assumptions and simplifications that may affect the calculated photocurrent densities and current mismatch. In the current match calculations, it was assumed that the perovskite sub-cell absorbs all incident photons transmitted to it, with no losses other than the modelled front-side absorption. Therefore, the external quantum efficiency (EQE) of the perovskite sub-cell was assumed to be 1. This simplified approach was used as there were no available EQE data and optical properties for the same perovskite structure in the literature at the time of the study. Ideally, these properties should be for an identical structure to ensure consistency. The simplified setup most likely overestimates perovskite photocurrent density production, as there are no losses included for perovskite sub-cell. Additionally, the transmitted fraction of light,

representing the photons passing through the perovskite sub-cell, was assumed to be the only optical loss between the sub-cells. In reality, additional losses such as reflection, scattering, and parasitic absorption are present when the cell operates under real-world conditions.

To ensure consistency, the EQE and optical data should ideally be for the same device, as EQE is device specific rather than material specific. In this study, such matching data were not available. As a result, the optical properties of a less commonly used perovskite (FACs)PbBr3-perovskite together with a PERC silicon sub-cell were used, which was the best available approximation for the tandem structure. The optical properties of the silicon sub-cell were based on the EQE of a silicon heterojunction (SHJ) cell. This simplification is not expected to significantly affect the results, as the transmitted photons were assumed to depend only on the perovskite sub-cell. Thus, the silicon sub-cell represents a generic bottom cell rather than a specific cell architecture.

In this study, optical losses were simplified, as the main focus was on the behaviour of the sub-cells under different weather conditions and seasons, specifically in terms of current matching rather than on absolute photocurrent values. For future work, the optical modelling could be made in more detail, by including full cell structures and considering the additional optical losses mentioned above, which would improve the accuracy of these absolute current match calculations.

No electrical losses were included in the current matching calculations either, as the focus of this study was on the spectral behaviour of the sub-cells. In real-world operation, electrical losses such as losses in open-circuit voltage V_{oc} or fill factor losses, and recombination can reduce the tandem photocurrent. Additionally, outside conditions or degradation of the sub-cells were not included in this model. Degradation is likely to occur at least in the perovskite-sub cell due to its shorter lifetime and instability, which can affect the overall efficiency of the tandem device. Outside conditions, such as temperature, can affect the current matching conditions. In addition to degradation and outside conditions, layer thicknesses of the sub-cells were not considered, which can affect the sub-cell's photocurrents significantly.

To improve the accuracy of future calculations, measured EQE data for both sub-cells under the same conditions could be used instead of simplified assumptions, and electrical losses could be included into the model. Additionally, in future work the layer thicknesses, especially tuning the perovskite layer, could be modelled or experimentally measured to see how it affects the current match. This would allow to determine the ideal band gap combinations in a specific

location, for instance in Finland. Another important aspect to consider is the use of more realistic device configurations. In this work, the optical properties and EQE data were from different silicon cell architectures (PERC and SHJ), which introduces unreliability. Future studies could address this by using matched data for a specific device structure, such as an SHJ silicon sub-cell combined with more commonly used perovskite absorber.

5.5 Outlook of Perovskite-Silicon Tandem Solar Cells

Besides optimizing the tandem modelling using more accurate EQE data and more detailed modelling approaches discussed in the previous section, further research is needed to fully understand the factors influencing current matching and to optimize the matching conditions in perovskite-silicon tandem solar cells (PSTSCs). As mentioned earlier, researchers have suggested optimizing the layer thicknesses [21],[57],[99], especially in the perovskite layer, to enhance the operation of PSTSCs under different conditions. This could be done by tuning the perovskite layer to optimize the light absorption for a specific geographical location.

Additionally, luminescent coupling has been researched to mitigate the current mismatch phenomenon of PSTSCs [109],[110]. Recent studies have shown that luminescent coupling (LC) can increase the possible band gap options and layer thicknesses, as well as mitigate the effects of spectral variations [110]. LC is particularly useful when the higher band gap perovskite-cell produces more current than the lower silicon sub-cell [109], as was the case in this thesis. With luminescent coupling, excess current of the perovskite sub-cell does not get lost, but can be partially re-emitted as photons absorbed by the silicon sub-cell [110], thereby providing an alternative way to reduce the current matching requirement of PSTSCs. Future work could therefore focus on ways to enhance luminescent coupling, for instance by tuning perovskite's properties to be more luminescent or by enhancing the optical transparency between the sub-cells.

Besides performance optimization, the commercialization of PSTSCs is still hindered by the limited long-term stability of perovskite solar cells. Degradation induced by environmental factors such as moisture and oxygen continue to be a major challenge. Promising strategies to address this issue include compositional engineering of perovskite toward intrinsically more stable structures, as well as encapsulation approaches to prevent the ingress of external factors, such as moisture and oxygen, for entering the device. At the time of this study, no literature was found that evaluates how degradation affects current matching or how current mismatch accelerates degradation in PSTSCs. Some studies suggest that current mismatch may enhance

degradation [60], but no specific rates were found, indicating a clear gap in the current literature. Progress in these areas will be an essential step towards the commercial availability of perovskite solar cells, and therefore tandem structures like PSTSCs.

6 Conclusions

Tandem solar cells have attracted considerable interest in recent years, as conventional silicon solar cells are approaching their theoretical maximum efficiencies. Tandem solar cells utilize multiple single-junction solar cells to form a highly efficient solar cell. Perovskite-silicon tandem solar cells (PSTSCs) combine both perovskite cells, with a high band gap, and silicon cells, with a lower band gap, which enables the tandem cells to absorb different wavelength ranges. Despite the promising efficiency of PSTSCs, many aspects still need to be developed before these cells can be used commercially.

One of the most important contributing factors is the instability of perovskite. This causes the perovskite sub-cell to have a limited operating life, and consequently the overall lifetime of the tandem cell. In this thesis, the stability challenges are addressed through a literature review, examining reported studies of the aging of PSTSCs. The literature review indicates that further research is needed for PSTSCs, particularly in terms of the effects of light and UV-light exposure. Many existing studies are limited to short-term testing, which cannot reliably predict real-life operation. Additionally, some studies used unencapsulated tandem cells, even though encapsulation is essential for improving device lifetime and the stability of perovskite sub-cells. Overall, the reviewed aging studies indicated that more long-term testing is needed, particularly to study the effects of UV and visible light. To ensure that laboratory results are comparable to outdoor operation, testing durations of at least 1000 hours are required. This highlights the need for standardized testing protocols for PSTSCs.

Besides stability concerns, spectral variations represent a significant research area needing further attention for PSTSCs. In this context, one of the key consequences of spectral variation is current mismatch, which strongly affects the operation of tandem cells. It refers to a situation in which the sub-cells do not produce the same current at the same time. The current-matching phenomenon has received relatively limited attention, and existing studies are often conducted under laboratory conditions. However, such conditions do not accurately represent real-life operation, as outdoor illumination varies with time of the day and season. Therefore, in this thesis the current match conditions in PSTSCs were analysed based on a review from existing spectral studies and a modelling approach applied to outdoor irradiance data.

The results highlighted that the absolute current mismatch increased with irradiance throughout the different days compared across all seasons, as higher irradiance led to higher photocurrent

densities in the sub-cells. The average current mismatch value during the measurement period was found to be around 2.8 mA/cm², indicating that the perovskite sub-cell produced more photocurrent overall. This can partly be explained by the simplified assumptions regarding the optical losses of the modelled tandem device, likely overestimating photocurrent production of the perovskite sub-cell. Additionally, current matching showed greater variability on cloudy days, whereas clear days produced smoother curves and more regular daily trends, which may be due to higher variability of the incoming sunlight during the cloudy days. The ratio of sub-cell photocurrent densities, which indicates relative current match, increased near midday, while higher variability was often observed in the mornings and evenings, indicating differences in the sub-cell photocurrent generation during these times. Throughout the measurement period, the perovskite sub-cell was generally the sub-cell producing more photocurrent, with only a few periods (early mornings and late evenings) where the silicon sub-cell produced slightly more.

Due to the lack of available material for detailed current match calculations, these calculations were performed using a simplified and straightforward method. Future studies could improve the accuracy of the calculations by including more detailed sub-cell properties as well as optical and electrical losses. Additionally, in future studies, the tandem cell could consist of an SHJ silicon sub-cell combined with an optimally band gapped perovskite sub-cell. Improved current matching could be achieved by tuning the perovskite absorber layer, for example by tuning its band gap or thickness, to allow more photons to reach the silicon sub-cell. Furthermore, approaches including luminescent coupling and tuning the perovskite sub-cell for different geographical locations could provide effective ways to reduce current mismatch in perovskite-silicon tandem solar cells.

References

[1] Y. Shi, J. J. Berry, and F. Zhang, “Perovskite/Silicon Tandem Solar Cells: Insights and Outlooks,” *ACS Energy Lett.*, vol. 9, no. 3, pp. 1305–1330, Mar. 2024, doi: 10.1021/ACSENERGYLETT.4C00172.

[2] F. Fu *et al.*, “Monolithic Perovskite-Silicon Tandem Solar Cells: From the Lab to Fab?,” *Advanced Materials*, vol. 34, no. 24, p. 2106540, Jun. 2022, doi: 10.1002/ADMA.202106540.

[3] B. Chen *et al.*, “Insights into the Development of Monolithic Perovskite/Silicon Tandem Solar Cells,” *Adv. Energy Mater.*, vol. 12, no. 4, p. 2003628, Jan. 2022, doi: 10.1002/AENM.202003628;REQUESTEDJOURNAL:JOURNAL:16146840;ISSUE:ISSUE:DOI.

[4] F. Hou *et al.*, “Monolithic perovskite/silicon tandem solar cells: A review of the present status and solutions toward commercial application,” *Nano Energy*, vol. 124, p. 109476, Jun. 2024, doi: 10.1016/J.NANOEN.2024.109476.

[5] R. K. Raman, S. A. Gurusamy Thangavelu, S. Venkataraj, and A. Krishnamoorthy, “Materials, methods and strategies for encapsulation of perovskite solar cells: From past to present,” *Renewable and Sustainable Energy Reviews*, vol. 151, p. 111608, Nov. 2021, doi: 10.1016/J.RSER.2021.111608.

[6] S. Akhil *et al.*, “Review on perovskite silicon tandem solar cells: Status and prospects 2T, 3T and 4T for real world conditions,” *Mater. Des.*, vol. 211, p. 110138, Dec. 2021, doi: 10.1016/J.MATDES.2021.110138.

[7] S. A. U. Hasan, M. A. Zahid, S. Park, and J. Yi, “Stability Challenges for a Highly Efficient Perovskite/Silicon Tandem Solar Cell: A Review,” *Solar RRL*, vol. 8, no. 6, p. 2300967, Mar. 2024, doi: 10.1002/SOLR.202300967.

[8] “Standard Solar Spectra | PVEducation.” Accessed: Nov. 03, 2025. [Online]. Available: https://www.pveducation.org/pvcdrom/appendices/standard-solar-spectra

[9] M. Haider and J. L. Yang, “Efficient and stable perovskite–silicon two-terminal tandem solar cells,” *Rare Metals*, vol. 39, no. 7, pp. 745–747, Jul. 2020, doi: 10.1007/S12598-020-01430-4/FIGURES/1.

[10] M. Adnan, Z. Irshad, and J. Lim, “Impact of structural advancements interface engineering operational stability and commercial viability of perovskite/silicon tandem solar cells,” *Solar Energy*, vol. 286, p. 113190, Jan. 2025, doi: 10.1016/J.SOLENER.2024.113190.

[11] R. Li, R. Gong, H. Lin, M. A. Green, and D. Lan, “Reverse-bias challenges facing perovskite-silicon tandem solar cells under field conditions,” *Newton*, vol. 1, no. 1, p. 100001, Mar. 2025, doi: 10.1016/J.NEWTON.2024.100001.

[12] C. Ballif, F. J. Haug, M. Boccard, P. J. Verlinden, and G. Hahn, “Status and perspectives of crystalline silicon photovoltaics in research and industry,” *Nat. Rev. Mater.*, vol. 7, no. 8, pp. 597–616, Aug. 2022, doi: 10.1038/S41578-022-00423-2;SUBJMETA.

[13] M. Jošt, L. Kegelmann, L. Korte, and S. Albrecht, “Monolithic Perovskite Tandem Solar Cells: A Review of the Present Status and Advanced Characterization Methods Toward 30% Efficiency,” *Adv. Energy Mater.*, vol. 10, no. 26, p. 1904102, Jul. 2020, doi: 10.1002/AENM.201904102;REQUESTEDJOURNAL:JOURNAL:16146840;WGROUP:STRING:PUBLICATION.

[14] A. Machín and F. Márquez, “Advancements in Photovoltaic Cell Materials: Silicon, Organic, and Perovskite Solar Cells,” *Materials 2024, Vol. 17, Page 1165*, vol. 17, no. 5, p. 1165, Mar. 2024, doi: 10.3390/MA17051165.

[15] M. Di Sabatino, R. Hendawi, and A. S. Garcia, “Silicon Solar Cells: Trends, Manufacturing Challenges, and AI Perspectives,” *Crystals 2024, Vol. 14, Page 167*, vol. 14, no. 2, p. 167, Feb. 2024, doi: 10.3390/CRYST14020167.

[16] R. Vidal, J. A. Alberola-Borràs, N. Sánchez-Pantoja, and I. Mora-Seró, “Comparison of Perovskite Solar Cells with other Photovoltaics Technologies from the Point of View of Life Cycle Assessment,” *Advanced Energy and Sustainability Research*, vol. 2, no. 5, p. 2000088, May 2021, doi: 10.1002/AESR.202000088;SUBPAGE:STRING:FULL.

[17] M. I. Asghar, J. Zhang, H. Wang, and P. D. Lund, “Device stability of perovskite solar cells – A review,” *Renewable and Sustainable Energy Reviews*, vol. 77, pp. 131–146, Sep. 2017, doi: 10.1016/J.RSER.2017.04.003.

[18] S. Bhattarai *et al.*, “A detailed review of perovskite solar cells: Introduction, working principle, modelling, fabrication techniques, future challenges,” *Micro*

and Nanostructures, vol. 172, p. 207450, Dec. 2022, doi: 10.1016/J.MICRNA.2022.207450.

[19] "Silicon-Based Tandem Solar Cells and Modules - Fraunhofer ISE." Accessed: Jan. 12, 2026. [Online]. Available: https://www.ise.fraunhofer.de/en/business-areas/photovoltaics-materials-cells-and-modules/silicon-based-tandem-solar-cells-and-modules.html

[20] M. Jošt, L. Kegelmann, L. Korte, and S. Albrecht, "Monolithic Perovskite Tandem Solar Cells: A Review of the Present Status and Advanced Characterization Methods Toward 30% Efficiency," *Adv. Energy Mater.*, vol. 10, no. 26, p. 101076, Jul. 2020, doi: 10.1002/aenm.201904102.

[21] M. H. Futscher and B. Ehrler, "Efficiency Limit of Perovskite/Si Tandem Solar Cells," *ACS Energy Lett.*, vol. 1, no. 4, pp. 863–868, Oct. 2016, doi: 10.1021/ACSENERGYLETT.6B00405.

[22] Y. Wang, Y. Wang, F. Gao, and D. Yang, "Efficient Monolithic Perovskite/Silicon Tandem Photovoltaics," *Energy & Environmental Materials*, vol. 7, no. 3, p. e12639, May 2024, doi: 10.1002/EEM2.12639.

[23] "Best Research-Cell Efficiency Chart | Photovoltaic Research | NREL." Accessed: Sep. 09, 2025. [Online]. Available: https://www.nrel.gov/pv/cell-efficiency

[24] Z. Hu, C. Ran, H. Zhang, L. Chao, Y. Chen, and W. Huang, "The Current Status and Development Trend of Perovskite Solar Cells," *Engineering*, vol. 21, pp. 15–19, Feb. 2023, doi: 10.1016/J.ENG.2022.10.012.

[25] B. Aïssa *et al.*, "Impact of the oxygen content on the optoelectronic properties of the indium-tin-oxide based transparent electrodes for silicon heterojunction solar cells," *AIP Conf. Proc.*, vol. 2147, Aug. 2019, doi: 10.1063/1.5123827.

[26] J. X. Song, X. X. Yin, Z. F. Li, and Y. W. Li, "Low-temperature-processed metal oxide electron transport layers for efficient planar perovskite solar cells," *Rare Metals*, vol. 40, no. 10, pp. 2730–2746, Oct. 2021, doi: 10.1007/S12598-020-01676-Y.

[27] Z. Ying, X. Yang, X. Wang, and J. Ye, "Towards the 10-Year Milestone of Monolithic Perovskite/Silicon Tandem Solar Cells," *Advanced Materials*, vol. 36, no. 37, p. 2311501, Sep. 2024, doi: 10.1002/ADMA.202311501;CSUBTYPE:STRING:SPECIAL;PAGE:STRING:ARTICLE/CHAPTER.

[28] R. Sharma, A. Sharma, S. Agarwal, and M. S. Dhaka, “Stability and efficiency issues, solutions and advancements in perovskite solar cells: A review,” *Solar Energy*, vol. 244, pp. 516–535, Sep. 2022, doi: 10.1016/J.SOLENER.2022.08.001.

[29] S. Guruprasad, A. Malik, A. Saidarsan, P. Basumatary, and D. S. Ghosh, “Modeling optical losses in perovskite solar cells: A modified framework toward realistic performance projection,” *Solar Energy*, vol. 305, p. 114251, Feb. 2026, doi: 10.1016/J.SOLENER.2025.114251.

[30] S. M. M. Y. C.-S. J. J. Y. H. E.-C. J. Chowdhury, “Electrical Loss Reduction in Crystalline Silicon Photovoltaic Module Assembly: A Review,” *Current Photovoltaic Research*, vol. 7, no. 4, pp. 111–120, 2019, doi: 10.21218/CPR.2019.7.4.111.

[31] J. Chen and N. G. Park, “Causes and Solutions of Recombination in Perovskite Solar Cells,” *Advanced Materials*, vol. 31, no. 47, p. 1803019, Nov. 2019, doi: 10.1002/adma.201803019.

[32] M. Tao *et al.*, “Major challenges and opportunities in silicon solar module recycling,” *Progress in Photovoltaics: Research and Applications*, vol. 28, no. 10, pp. 1077–1088, Oct. 2020, doi: 10.1002/PIP.3316;WGROUP:STRING:PUBLICATION.

[33] E. S. Akulenko, M. Hadadian, A. Santasalo-Aarnio, and K. Miettunen, “Eco-design for perovskite solar cells to address future waste challenges and recover valuable materials,” *Heliyon*, vol. 9, no. 2, p. e13584, Feb. 2023, doi: 10.1016/j.heliyon.2023.e13584.

[34] L. Mazzarella *et al.*, “Infrared Light Management Using a Nanocrystalline Silicon Oxide Interlayer in Monolithic Perovskite/Silicon Heterojunction Tandem Solar Cells with Efficiency above 25%,” *Adv. Energy Mater.*, vol. 9, no. 14, p. 1803241, Apr. 2019, doi: 10.1002/AENM.201803241;PAGEGROUP:STRING:PUBLICATION.

[35] Y. Cheng and L. Ding, “Perovskite/Si tandem solar cells: Fundamentals, advances, challenges, and novel applications,” *SusMat*, vol. 1, no. 3, pp. 324–344, Sep. 2021, doi: 10.1002/SUS2.25.

[36] K. J. Weber, K. R. Catchpole, D. T. Grant, and T. P. White, “Design guidelines for perovskite/silicon 2-terminal tandem solar cells: an optical study,” *Optics*

Express, Vol. 24, Issue 22, pp. A1454-A1470, vol. 24, no. 22, pp. A1454–A1470, Oct. 2016, doi: 10.1364/OE.24.0A1454.

[37] S. Bhattarai *et al.*, "A detailed review of perovskite solar cells: Introduction, working principle, modelling, fabrication techniques, future challenges," *Micro and Nanostructures*, vol. 172, p. 207450, Dec. 2022, doi: 10.1016/j.micrna.2022.207450.

[38] J. Huang and L. Mao, "A Review on Perovskite/Silicon Tandem Solar Cells: Current Status and Future Challenges," *Energies 2025, Vol. 18, Page 4327*, vol. 18, no. 16, p. 4327, Aug. 2025, doi: 10.3390/en18164327.

[39] M. De Bastiani, A. S. Subbiah, E. Aydin, F. H. Isikgor, T. G. Allen, and S. De Wolf, "Recombination junctions for efficient monolithic perovskite-based tandem solar cells: physical principles, properties, processing and prospects," *Mater. Horiz.*, vol. 7, no. 11, pp. 2791–2809, Nov. 2020, doi: 10.1039/d0mh00990c.

[40] R. Wang, M. Mujahid, Y. Duan, Z. K. Wang, J. Xue, and Y. Yang, "A Review of Perovskites Solar Cell Stability," *Adv. Funct. Mater.*, vol. 29, no. 47, p. 1808843, Nov. 2019, doi: 10.1002/ADFM.201808843.

[41] L. Xiang *et al.*, "Progress on the stability and encapsulation techniques of perovskite solar cells," *Org. Electron.*, vol. 106, p. 106515, Jul. 2022, doi: 10.1016/J.ORGEL.2022.106515.

[42] M. I. Asghar, J. Zhang, H. Wang, and P. D. Lund, "Device stability of perovskite solar cells – A review," *Renewable and Sustainable Energy Reviews*, vol. 77, pp. 131–146, Sep. 2017, doi: 10.1016/J.RSER.2017.04.003.

[43] D. Wang, M. Wright, N. K. Elumalai, and A. Uddin, "Stability of perovskite solar cells," *Solar Energy Materials and Solar Cells*, vol. 147, pp. 255–275, Apr. 2016, doi: 10.1016/J.SOLMAT.2015.12.025.

[44] C. C. Boyd, R. Cheacharoen, T. Leijtens, and M. D. McGehee, "Understanding Degradation Mechanisms and Improving Stability of Perovskite Photovoltaics," *Chem. Rev.*, vol. 119, no. 5, pp. 3418–3451, Mar. 2018, doi: 10.1021/ACS.CHEMREV.8B00336.

[45] L. Mu *et al.*, "Innovative Materials for Lamination Encapsulation in Perovskite Solar Cells," *Adv. Funct. Mater.*, vol. 35, no. 7, p. 2415353, Feb. 2025, doi: 10.1002/ADFM.202415353.

[46] H. Jiao *et al.*, “Metal Halide Perovskite Solar Module Encapsulation Using Polyolefin Elastomers: The Role of Morphology in Preventing Delamination,” *PRX Energy*, vol. 3, no. 2, p. 023013, Jun. 2024, doi: 10.1103/PRXEnergy.3.023013.

[47] R. K. Raman, S. Ganesan, A. Alagumalai, V. Sudhakaran Menon, S. A. Gurusamy Thangavelu, and A. Krishnamoorthy, “Rational Design, Synthesis, and Structure–Property Relationship Studies of a Library of Thermoplastic Polyurethane Films as an Effective and Scalable Encapsulation Material for Perovskite Solar Cells,” *ACS Appl. Mater. Interfaces*, vol. 15, no. 46, pp. 53935–53950, Nov. 2023, doi: 10.1021/ACSAMI.3C12607.

[48] A. Ndiaye, A. Charki, A. Kobi, C. M. F. Kébé, P. A. Ndiaye, and V. Sambou, “Degradations of silicon photovoltaic modules: A literature review,” *Solar Energy*, vol. 96, pp. 140–151, Oct. 2013, doi: 10.1016/J.SOLENER.2013.07.005.

[49] O. K. Segbefia, N. Akhtar, and T. O. Sætre, “Moisture induced degradation in field-aged multicrystalline silicon photovoltaic modules,” *Solar Energy Materials and Solar Cells*, vol. 258, p. 112407, Aug. 2023, doi: 10.1016/J.SOLMAT.2023.112407.

[50] W. Luo *et al.*, “Potential-induced degradation in photovoltaic modules: a critical review,” *Energy Environ. Sci.*, vol. 10, no. 1, pp. 43–68, Jan. 2017, doi: 10.1039/c6ee02271e.

[51] L. Ning, L. Song, and J. Zhang, “Research progress of light and elevated temperature-induced degradation in silicon solar cells: A review,” *J. Alloys Compd.*, vol. 912, p. 165120, Aug. 2022, doi: 10.1016/J.JALLCOM.2022.165120.

[52] H. Shamachurn and T. Betts, “Experimental Study of the Degradation of Silicon Photovoltaic Devices under Ultraviolet Radiation Exposure,” *Journal of Solar Energy*, vol. 2016, no. 1, p. 2473245, Jan. 2016, doi: 10.1155/2016/2473245.

[53] A. Sinha *et al.*, “UV-induced degradation of high-efficiency silicon PV modules with different cell architectures,” *Progress in Photovoltaics: Research and Applications*, vol. 31, no. 1, pp. 36–51, Jan. 2023, doi: 10.1002/PIP.3606.

[54] D. Yang *et al.*, “28.3%-efficiency perovskite/silicon tandem solar cell by optimal transparent electrode for high efficient semitransparent top cell,” *Nano Energy*, vol. 84, p. 105934, Jun. 2021, doi: 10.1016/J.NANOEN.2021.105934.

[55] A. Kumar, S. Singh, M. K. A. Mohammed, and A. E. Shalan, “Computational Modelling of Two Terminal CIGS/Perovskite Tandem Solar Cells with Power Conversion Efficiency of 23.1 %,” *Eur. J. Inorg. Chem.*, vol. 2021, no. 47, pp. 4959–4969, Dec. 2021, doi: 10.1002/ejic.202100214.

[56] H. Bristow *et al.*, “Mitigating Delamination in Perovskite/Silicon Tandem Solar Modules,” *Solar RRL*, vol. 8, no. 14, p. 2400289, Jul. 2024, doi: 10.1002/SOLR.202400289.

[57] N. Shrivastav, J. Madan, R. Pandey, and A. E. Shalan, “Investigations aimed at producing 33% efficient perovskite–silicon tandem solar cells through device simulations,” *RSC Adv.*, vol. 11, no. 59, pp. 37366–37374, Nov. 2021, doi: 10.1039/D1RA06250F.

[58] J. Qian *et al.*, “Destructive reverse bias pinning in perovskite/ silicon tandem solar modules caused by perovskite hysteresis under dynamic shading †,” 2020, doi: 10.1039/c9se01246j.

[59] S. Akhil *et al.*, “Review on perovskite silicon tandem solar cells: Status and prospects 2T, 3T and 4T for real world conditions,” *Mater. Des.*, vol. 211, p. 110138, Dec. 2021, doi: 10.1016/J.MATDES.2021.110138.

[60] E. Köhnen *et al.*, “Highly efficient monolithic perovskite silicon tandem solar cells: analyzing the influence of current mismatch on device performance,” *Sustain. Energy Fuels*, vol. 3, no. 8, pp. 1995–2005, Jul. 2019, doi: 10.1039/C9SE00120D.

[61] H. Raza *et al.*, “Potential-induced degradation: a challenge in the commercialization of perovskite solar cells,” *Energy Environ. Sci.*, vol. 17, no. 5, pp. 1819–1853, Mar. 2024, doi: 10.1039/d3ee03317a.

[62] L. Xu *et al.*, “Potential-induced degradation in perovskite/silicon tandem photovoltaic modules,” *Cell Rep. Phys. Sci.*, vol. 3, no. 9, p. 101026, Sep. 2022, doi: 10.1016/j.xcrp.2022.101026.

[63] A. A. Q. Hasan *et al.*, “A review on silicon photovoltaic module degradations and recent identification techniques,” *Solar Energy*, vol. 288, p. 113288, Mar. 2025, doi: 10.1016/J.SOLENER.2025.113288.

[64] M. R. Maghami, H. Hizam, C. Gomes, M. A. Radzi, M. I. Rezadad, and S. Hajighorbani, “Power loss due to soiling on solar panel: A review,” *Renewable and Sustainable Energy Reviews*, vol. 59, pp. 1307–1316, Jun. 2016, doi: 10.1016/J.RSER.2016.01.044.

[65] L. Guanghua, A. M. Soomar, S. H. H. Shah, S. Shaikh, and P. Musznicki, "Maximum power point tracking strategies for solar PV systems: A review of current methods and future innovations," *Results in Engineering*, vol. 28, p. 107227, Dec. 2025, doi: 10.1016/J.RINENG.2025.107227.

[66] K. A. Bush *et al.*, "23.6%-efficient monolithic perovskite/silicon tandem solar cells with improved stability," *Nat. Energy*, vol. 2, no. 4, pp. 1–7, Mar. 2017, doi: 10.1038/NENERGY.2017.9;SUBJMETA=4077,4096,4101,639,909,946;KWRD=SOLAR+CELLS.

[67] F. Toniolo *et al.*, "Efficient and reliable encapsulation for perovskite/silicon tandem solar modules," *Nanoscale*, vol. 15, no. 42, pp. 16984–16991, Nov. 2023, doi: 10.1039/D2NR06873G.

[68] R. Cheacharoen *et al.*, "Encapsulating perovskite solar cells to withstand damp heat and thermal cycling †," 2018, doi: 10.1039/c8se00250a.

[69] M. De Bastiani *et al.*, "Toward Stable Monolithic Perovskite/Silicon Tandem Photovoltaics: A Six-Month Outdoor Performance Study in a Hot and Humid Climate," *ACS Energy Lett.*, vol. 6, pp. 2944–2951, 2021, doi: 10.1021/ACSENERGYLETT.1C01018/ASSET/IMAGES/LARGE/NZ1C01018_0004.JPEG.

[70] J. Liu *et al.*, "Efficient and stable perovskite-silicon tandem solar cells through contact displacement by MgFx," *Science (1979).*, vol. 377, no. 6603, pp. 302–306, Jun. 2022, doi: 10.1126/SCIENCE.ABN8910.

[71] Y. Hou *et al.*, "Efficient tandem solar cells with solution-processed perovskite on textured crystalline silicon," *Science (1979).*, vol. 367, no. 6482, pp. 1135–1140, Mar. 2020, doi: 10.1126/SCIENCE.AAY0262.

[72] A. Al-Ashouri *et al.*, "Monolithic perovskite/silicon tandem solar cell with >29% efficiency by enhanced hole extraction," *Science (1979).*, vol. 370, no. 6522, pp. 1300–1309, Dec. 2020, doi: 10.1126/SCIENCE.ABD4016/SUPPL_FILE/ABD4016_AL-ASHOURI_SM.PDF.

[73] J. Liu *et al.*, "28.2%-efficient, outdoor-stable perovskite/silicon tandem solar cell," *Joule*, vol. 5, no. 12, pp. 3169–3186, Dec. 2021, doi: 10.1016/j.joule.2021.11.003.

[74] H. Luo *et al.*, “Damp-Stable Perovskite/Silicon Tandem Solar Cells with Internal Encapsulating Sulfonium-Based Molecules,” *ACS Energy Lett.*, vol. 10, no. 7, pp. 3325–3334, Jul. 2025, doi: 10.1021/ACSENERGYLETT.5C01010.

[75] “Solar Spectra - an overview | ScienceDirect Topics.” Accessed: Nov. 03, 2025. [Online]. Available: https://www.sciencedirect.com/topics/physics-and-astronomy/solar-spectra

[76] G. S. Kinsey *et al.*, “Impact of measured spectrum variation on solar photovoltaic efficiencies worldwide,” *Renew. Energy*, vol. 196, pp. 995–1016, Aug. 2022, doi: 10.1016/J.RENENE.2022.07.011.

[77] A. Andreas and T. Stoffel, “NREL Solar Radiation Research Laboratory (SRRL): Baseline Measurement System (BMS); Golden, Colorado (Data); NREL Report No. DA-5500-56488.” Accessed: Nov. 20, 2025. [Online]. Available: http://dx.doi.org/10.5439/1052221

[78] S. W. Director *et al.*, “Solar cells - From Basics to Advanced Systems,” in *McGraw-Hill Series in Electrical Engineering*, 1983.

[79] “Atmospheric Effects | PVEducation.” Accessed: Nov. 04, 2025. [Online]. Available: https://www.pveducation.org/pvcdrom/properties-of-sunlight/atmospheric-effects

[80] T. M. Yunus Khan *et al.*, “Optimum location and influence of tilt angle on performance of solar PV panels,” *J. Therm. Anal. Calorim.*, vol. 141, no. 1, pp. 511–532, Jul. 2020, doi: 10.1007/S10973-019-09089-5/FIGURES/24.

[81] H. Y. Cheng, C. C. Yu, K. C. Hsu, C. C. Chan, M. H. Tseng, and C. L. Lin, “Estimating Solar Irradiance on Tilted Surface with Arbitrary Orientations and Tilt Angles,” *Energies 2019, Vol. 12, Page 1427*, vol. 12, no. 8, p. 1427, Apr. 2019, doi: 10.3390/EN12081427.

[82] A. K. Yadav and S. S. Chandel, “Tilt angle optimization to maximize incident solar radiation: A review,” *Renewable and Sustainable Energy Reviews*, vol. 23, pp. 503–513, Jul. 2013, doi: 10.1016/J.RSER.2013.02.027.

[83] Z. K. Pecenak, F. A. Mejia, B. Kurtz, A. Evan, and J. Kleissl, “Simulating irradiance enhancement dependence on cloud optical depth and solar zenith angle,” *Solar Energy*, vol. 136, pp. 675–681, Oct. 2016, doi: 10.1016/J.SOLENER.2016.07.045.

[84] S. Acharyya *et al.*, “Dopant-free materials for carrier-selective passivating contact solar cells: A review,” *Surfaces and Interfaces*, vol. 28, p. 101687, Feb. 2022, doi: 10.1016/J.SURFIN.2021.101687.

[85] E. Aydin *et al.*, “Pathways toward commercial perovskite/silicon tandem photovoltaics,” *Science (1979).*, vol. 383, no. 6679, pp. 1–13, Jan. 2024, doi: 10.1126/SCIENCE.ADH3849.

[86] E. Aydin *et al.*, “Interplay between temperature and bandgap energies on the outdoor performance of perovskite/silicon tandem solar cells,” *Nat. Energy*, vol. 5, no. 11, pp. 851–859, Nov. 2020, doi: 10.1038/S41560-020-00687-4;SUBJMETA.

[87] S. Wu, C. Li, S. Y. Lien, and P. Gao, “Temperature Matters: Enhancing Performance and Stability of Perovskite Solar Cells through Advanced Annealing Methods,” *Chemistry 2024, Vol. 6, Pages 207-236*, vol. 6, no. 1, pp. 207–236, Jan. 2024, doi: 10.3390/CHEMISTRY6010010.

[88] C. Wang *et al.*, “Perovskite Solar Cells in the Shadow: Understanding the Mechanism of Reverse-Bias Behavior toward Suppressed Reverse-Bias Breakdown and Reverse-Bias Induced Degradation,” *Adv. Energy Mater.*, vol. 13, no. 9, p. 2203596, Mar. 2023, doi: 10.1002/AENM.202203596.

[89] D. Bogachuk and F. Feldmann, “Do perovskites need silicon to be stable under reverse bias?,” *Joule*, vol. 7, no. 11, pp. 2423–2426, Nov. 2023, doi: 10.1016/j.joule.2023.10.017.

[90] J. Kusuma and R. Geetha Balakrishna, “A review on electrical characterization techniques performed to study the device performance of quantum dot sensitized solar cells,” *Solar Energy*, vol. 159, pp. 682–696, Jan. 2018, doi: 10.1016/J.SOLENER.2017.11.037.

[91] A. Alheloo *et al.*, “Quantum efficiency as a tool for defect analysis in solar photovoltaic modules,” *Renewable Energy Production and Distribution: Solutions and Opportunities: Volume 2*, vol. 2, pp. 111–142, Jan. 2023, doi: 10.1016/B978-0-443-18439-0.00001-X.

[92] N. Ali *et al.*, “Beyond lead: Progress in stable and non-toxic lower-dimensional perovskites for high-performance photodetection,” *Sustainable Materials and Technologies*, vol. 38, p. e00759, Dec. 2023, doi: 10.1016/J.SUSMAT.2023.E00759.

[93] N. T. R. N. Kumara, A. Lim, C. M. Lim, M. I. Petra, and P. Ekanayake, "Recent progress and utilization of natural pigments in dye sensitized solar cells: A review," *Renewable and Sustainable Energy Reviews*, vol. 78, pp. 301–317, Oct. 2017, doi: 10.1016/J.RSER.2017.04.075.

[94] W. Ananda, "External quantum efficiency measurement of solar cell," *QiR 2017 - 2017 15th International Conference on Quality in Research (QiR): International Symposium on Electrical and Computer Engineering*, vol. 2017-December, pp. 450–456, Dec. 2017, doi: 10.1109/QIR.2017.8168528.

[95] D. Chojniak *et al.*, "Measuring the External Quantum Efficiency of Tandem Photovoltaic Modules Using an LED-Based Solar Simulator," *Solar RRL*, vol. 9, no. 1, p. 2400517, Jan. 2025, doi: 10.1002/SOLR.202400517;SUBPAGE:STRING:FULL.

[96] "IEC 60904-8 INTERNATIONAL STANDARD NORME INTERNATIONALE Photovoltaic devices-Part 8: Measurement of spectral responsivity of a photovoltaic (PV) device Dispositifs photovoltaïques-Partie 8: Mesure de la sensibilité spectrale d'un dispositif photovoltaïqu…," 2014, Accessed: Dec. 16, 2025. [Online]. Available: www.iec.ch

[97] T. Matsui, C. McDonald, A. Mirzehmet, J. McQueen, R. S. Bonilla, and H. Sai, "Monolithic Perovskite/Silicon Tandem Solar Cells Enabled by Multifunctional TiOx Interconnects," *Small*, vol. 21, no. 24, Jun. 2025, doi: 10.1002/SMLL.202500969.

[98] A. J. Bett *et al.*, "Spectrometric Characterization of Monolithic Perovskite/Silicon Tandem Solar Cells," *Solar RRL*, vol. 7, no. 2, Feb. 2023, doi: 10.1002/SOLR.202200948.

[99] R. Witteck, J. F. Geisz, E. L. Warren, and W. E. McMahon, "Spectral Effects on the Energy Harvesting Efficiency of Two- and Four-Terminal Tandem Photovoltaics," *Solar RRL*, vol. 8, no. 3, p. 2300782, Feb. 2024, doi: 10.1002/SOLR.202300782.

[100] E. Köhnen *et al.*, "Highly efficient monolithic perovskite silicon tandem solar cells: analyzing the influence of current mismatch on device performance †," *Sustainable Energy Fuels*, 2019, doi: 10.1039/c9se00120d.

[101] W. Shockley and H. J. Queisser, "Detailed Balance Limit of Efficiency of p-n Junction Solar Cells," *J. Appl. Phys.*, vol. 32, no. 3, pp. 510–519, Mar. 1961, doi: 10.1063/1.1736034.

[102] S. P. Philipps *et al.*, “Energy harvesting efficiency of III–V triple-junction concentrator solar cells under realistic spectral conditions,” *Solar Energy Materials and Solar Cells*, vol. 94, no. 5, pp. 869–877, May 2010, doi: 10.1016/j.solmat.2010.01.010.

[103] R. Daxini, K. S. Anderson, J. S. Stein, and M. Theristis, “Photovoltaic Module Spectral Mismatch Losses Due to Cell-Level EQE Variation,” *IEEE J. Photovolt.*, vol. 15, no. 3, pp. 458–464, 2025, doi: 10.1109/JPHOTOV.2025.3545820.

[104] M. C. Schubert *et al.*, “Industrial Production of Perovskite–Silicon Tandem Solar Cells: The Characterization Challenge,” *Solar RRL*, vol. 10, no. 3, p. e202500766, Feb. 2026, doi: 10.1002/solr.202500766.

[105] C. Hägglund, “Multiscale Optical Modeling of Perovskite-Si Tandem Solar Cells,” *Frontiers in Photonics*, vol. 3, p. 921438, Jul. 2022, doi: 10.3389/FPHOT.2022.921438/BIBTEX.

[106] T. Yang *et al.*, “One-stone-for-two-birds strategy to attain beyond 25% perovskite solar cells,” *Nature Communications 2023 14:1*, vol. 14, no. 1, pp. 1–10, Feb. 2023, doi: 10.1038/s41467-023-36229-1.

[107] Z. Xie *et al.*, “27%-efficiency silicon heterojunction cell with 98.6% cell-to-module ratio driving new momentum towards the 29.4% limit,” *Nature Communications 2025 16:1*, vol. 16, no. 1, pp. 1–11, Oct. 2025, doi: 10.1038/s41467-025-64465-0.

[108] “Open data - Finnish Meteorological Institute.” Accessed: Jan. 21, 2026. [Online]. Available: https://en.ilmatieteenlaitos.fi/open-data

[109] K. Nguyen *et al.*, “The Role of Luminescent Coupling in Monolithic Perovskite/Silicon Tandem Solar Cells,” *Small*, vol. 20, no. 46, p. 2403461, Nov. 2024, doi: 10.1002/smll.202403461.

[110] A. R. Bowman *et al.*, “Relaxed Current Matching Requirements in Highly Luminescent Perovskite Tandem Solar Cells and Their Fundamental Efficiency Limits,” *ACS Energy Lett.*, vol. 6, no. 2, pp. 612–620, Feb. 2021, doi: 10.1021/ACSENERGYLETT.0C02481.

7 Appendices

7.1 Appendix 1. Code for Current Match Calculation

```
import glob
import os
import pandas as pd
import numpy as np

# Physical constants
h = 6.62607015e-34
c = 2.99792458e8
q = 1.602176634e-19

def read_ms711_file(path):
    df_raw = pd.read_csv(path, sep='\t', header=None)

    # Extract date and time rows
    date_row = df_raw.iloc[0, 1:]  # skip first column
    time_row = df_raw.iloc[1, 1:]

    def clean_date(d):
        # Remove suffix like ".1", ".2", etc.
        return str(d).split('.')[0].strip()

    full_times = [
        f"{clean_date(date)} {str(time).strip()}"
        for date, time in zip(date_row, time_row)
        if pd.notna(date) and pd.notna(time)
    ]

    # Read irradiance data
    df_data = pd.read_csv(path, sep='\t', skiprows=16)
    df_data = df_data.dropna(axis=1, how='all')  # drop empty columns

    wl = df_data.iloc[:, 0].to_numpy()
    irr_data = df_data.iloc[:, 1:].to_numpy()

    # Convert W/m2/um → W/m2/nm
    irr_data = irr_data / 1000.0

    return wl, full_times, irr_data

def read_eqe_dual(path, sheet=0):
    df = pd.read_excel(path, sheet_name=sheet)
    df.columns = df.columns.str.strip()

    # Ensure there are at least 4 columns
    if df.shape[1] < 4:
        raise ValueError(f"EQE sheet has {df.shape[1]} columns, expected >= 4 with
layout: "
                         "'wavelength_pero, EQE_pero, wavelength_si, EQE_si'")

    # Extract the two pairs of columns and coerce to numeric
    df_pero = df.iloc[:, [0, 1]].copy()
    df_pero.columns = ['wavelength_nm', 'EQE_pero']
    df_pero['wavelength_nm'] = pd.to_numeric(df_pero['wavelength_nm'],
errors='coerce')
    df_pero['EQE_pero'] = pd.to_numeric(df_pero['EQE_pero'], errors='coerce')

    df_si = df.iloc[:, [2, 3]].copy()
    df_si.columns = ['wavelength_nm', 'EQE_si']
    df_si['wavelength_nm'] = pd.to_numeric(df_si['wavelength_nm'], errors='coerce')
    df_si['EQE_si'] = pd.to_numeric(df_si['EQE_si'], errors='coerce')
```

```
    # Drop rows where wavelength is NaN or EQE is NaN for that pair
    df_pero = df_pero.dropna(subset=['wavelength_nm']).reset_index(drop=True)
    df_pero = df_pero.dropna(subset=['EQE_pero']).reset_index(drop=True)

    df_si = df_si.dropna(subset=['wavelength_nm']).reset_index(drop=True)
    df_si = df_si.dropna(subset=['EQE_si']).reset_index(drop=True)

    # Clip to physical bounds [0,1]
    df_pero['EQE_pero'] = df_pero['EQE_pero'].clip(0.0, 1.0)
    df_si['EQE_si'] = df_si['EQE_si'].clip(0.0, 1.0)

    df_pero = (df_pero
               .groupby('wavelength_nm', as_index=False)['EQE_pero']
               .mean()
               .sort_values('wavelength_nm')
               .reset_index(drop=True))

    df_si = (df_si
             .groupby('wavelength_nm', as_index=False)['EQE_si']
             .mean()
             .sort_values('wavelength_nm')
             .reset_index(drop=True))
    return df_pero, df_si


def read_absorption(path, round_wl=False):
    """
    Read absorption/transmission/reflectance data and return clean, sorted, data
suitable for np.interp.
    - Clips values to [0,1].
    - Checks A+T+R sum and prints diagnostics.
    """
    df = pd.read_excel(path)
    # normalize column names
    df.columns = df.columns.str.strip()

    # Accept several possible column names by lowering and matching
    colmap = {c.lower(): c for c in df.columns}
    # required keys (case-insensitive)
    required = ['wavelength', 'absorbed', 'transmittance', 'reflectance']
    for rk in required:
        if rk not in colmap:
            raise KeyError(f"read_absorption: expected column like '{rk}' in
{path}, found: {df.columns.tolist()}")

    wl_col = colmap['wavelength']
    A_col  = colmap['absorbed']
    T_col  = colmap['transmittance']
    R_col  = colmap['reflectance']

    # Coerce to numeric and drop completely NaN rows
    df = df[[wl_col, A_col, T_col, R_col]].copy()
    df[wl_col] = pd.to_numeric(df[wl_col], errors='coerce')
    df[A_col]  = pd.to_numeric(df[A_col], errors='coerce')
    df[T_col]  = pd.to_numeric(df[T_col], errors='coerce')
    df[R_col]  = pd.to_numeric(df[R_col], errors='coerce')
    df = df.dropna(subset=[wl_col]).reset_index(drop=True)

    # Optionally round wavelength
    if round_wl:
        df[wl_col] = df[wl_col].round().astype(int)

    # Group duplicate wavelengths by averaging A, T, R
    grouped = (df
               .groupby(wl_col, as_index=False)
               .agg({A_col: 'mean', T_col: 'mean', R_col: 'mean'}))

    # Sort by wavelength ascending
```

```
    grouped = grouped.sort_values(wl_col).reset_index(drop=True)

    # Clip to [0,1]
    grouped[A_col] = grouped[A_col].clip(0.0, 1.0)
    grouped[T_col] = grouped[T_col].clip(0.0, 1.0)
    grouped[R_col] = grouped[R_col].clip(0.0, 1.0)

    lam_nm = grouped[wl_col].to_numpy()
    A_raw  = grouped[A_col].to_numpy()
    T_raw  = grouped[T_col].to_numpy()
    R_raw  = grouped[R_col].to_numpy()

    # Diagnostics: check energy conservation and wavelength coverage
    sum_atr = A_raw + T_raw + R_raw
    bad_idx = np.where(np.abs(sum_atr - 1.0) > 0.02)[0]  # tolerance 0.02
    if bad_idx.size > 0:
        print(f"Warning: {bad_idx.size} wavelength points deviate A+T+R from 1 by
>0.02 (first index example: {bad_idx[0]}).")
        # print a couple examples
        for ii in bad_idx[:5]:
            print(f"  wl={lam_nm[ii]} nm: A={A_raw[ii]:.4f}, T={T_raw[ii]:.4f},
R={R_raw[ii]:.4f}, sum={sum_atr[ii]:.4f}")

    # Print summary
    def mean_in_range(arr, wl, lo, hi):
        m = np.nan
        mask = (wl >= lo) & (wl <= hi)
        if mask.any():
            m = float(np.nanmean(arr[mask]))
        return m

    print(f"Absorption file: wavelengths {lam_nm.min()} - {lam_nm.max()} nm,
{lam_nm.size} unique points")
    print(f"Mean T (400-800 nm): {mean_in_range(T_raw, lam_nm, 400, 800):.4f}")
    print(f"Mean T (800-1100 nm): {mean_in_range(T_raw, lam_nm, 800, 1100):.4f}")
    print(f"Min/Max T overall: {T_raw.min():.4g} / {T_raw.max():.4g}")

    return lam_nm, A_raw, T_raw, R_raw

def compute_photon_flux(irr_W_m2_nm, wavelength_nm):
    lam_m = wavelength_nm * 1e-9
    E_photon = (h * c) / lam_m
    return irr_W_m2_nm / E_photon  # photons / (s·m²·nm)

def trapezoid(y, x):
    return np.sum((y[1:] + y[:-1]) * (x[1:] - x[:-1]) / 2.0)

def integrate_Jsc(eqe, phi, wl_nm, optical_factor=1.0):
    # Ensure increasing wavelength order
    idx = np.argsort(wl_nm)
    wl = wl_nm[idx]
    eqe = eqe[idx]
    phi = phi[idx]

    integrand = q * eqe * phi * optical_factor  # C / (s·m²·nm)
    Jsc_A_m2 = np.trapezoid(integrand, wl)          # integrate over nm

    return Jsc_A_m2 * 0.1   # A/m² → mA/cm²

def main():
    folder = r"filepath_name_here"

    # Find all .txt files in the folder
    files = glob.glob(os.path.join(folder, "*.txt"))

    # Load EQE and optical data once
    df_pero, df_si = read_eqe_dual("data/EQE.xlsx")
    lam_A_nm, A_raw, T_raw, R_raw = read_absorption("data/transmittance.xlsx")
```

```
    all_results = []

    # Loop through every file
    for filepath in files:
        wl_use, time_labels, irr_matrix = read_ms711_file(filepath)

        filename = os.path.basename(filepath)

        for i, time_label in enumerate(time_labels):
            # 1. Clip irradiance (remove negative noise)
            irr_total = np.clip(irr_matrix[:, i], 0.0, None)

            # 2. Restrict wavelengths to ≥ 300 nm
            mask = wl_use >= 300
            wl_filt = wl_use[mask]
            irr_filt = irr_total[mask]

            # 3. Compute photon flux using filtered data
            phi = compute_photon_flux(irr_filt, wl_filt)

            # 4. PEROVSKITE: EQE = 1, optical factor = absorbance
            EQE_pero = np.ones_like(wl_filt)
            A_front = np.interp(wl_filt, lam_A_nm, A_raw, left=0, right=0)
            Jsc_pero = integrate_Jsc(EQE_pero, phi, wl_filt,
optical_factor=A_front)

            # 5. SILICON: normal EQE and transmittance
            EQE_si = np.interp(wl_filt, df_si["wavelength_nm"], df_si["EQE_si"],
left=0, right=0)
            T_rear = np.interp(wl_filt, lam_A_nm, T_raw, left=0, right=0)
            Jsc_si = integrate_Jsc(EQE_si, phi, wl_filt, optical_factor=T_rear)

            # 6. Tandem = limiting subcell
            Jsc_tandem = min(Jsc_pero, Jsc_si)

            # 7. Store results
            all_results.append([
                filename,
                time_label,
                Jsc_pero,
                Jsc_si,
                Jsc_tandem
            ])

    # Save everything into Excel file
    df_out = pd.DataFrame(
        all_results,
        columns=["File", "Time", "Perovskite Jsc", "Silicon Jsc", "Tandem Jsc"]
    )

    # Convert Time to datetime
    dt = pd.to_datetime(df_out["Time"], format="%Y/%m/%d %H:%M:%S",
errors="coerce")

    # Create separate Date and Time columns
    df_out["Date"] = dt.dt.strftime("%Y-%m-%d")
    df_out["Clock"] = dt.dt.strftime("%H:%M")

    # Numeric hours for plotting (04.00, 04.08, 04.17...)
    df_out["Hour"] = dt.dt.hour + dt.dt.minute / 60

    # Reorder columns for clarity
    df_out = df_out[[
        "File", "Date", "Clock", "Hour",
        "Perovskite Jsc", "Silicon Jsc", "Tandem Jsc"
    ]]
```

```
    # Sort chronologically
    df_out = df_out.sort_values(["Date", "Clock"])

    df_out.to_excel("all_ms711_results.xlsx", index=False)

    output_path = os.path.abspath("all_ms711_results.xlsx")
    print("Saved results to:", output_path)

if __name__ == "__main__":
    main()
```